BRAIN
ORIGINAL ARTICLE

Interferon-γ controls aquaporin 4-specific Th17 and B cells in neuromyelitis optica spectrum disorder

Gabriel Arellano,[1,†] Eileah Loda,[2,†] Yanan Chen,[3] Tobias Neef,[1] Andrew C. Cogswell,[1] Grant Primer,[1] Godwin Joy,[3] Kevin Kaschke,[3] Samantha Wills,[3] Joseph R. Podojil,[1,4] Brian Popko,[2] Roumen Balabanov[2] and Stephen D. Miller[1]

[†]These authors contributed equally to this work.

Neuromyelitis optica spectrum disorder (NMOSD) is a CNS autoimmune inflammatory disease mediated by T helper 17 (Th17) and antibody responses to the water channel protein, aquaporin 4 (AQP4), and associated with astrocytopathy, demyelination and axonal loss. Knowledge about disease pathogenesis is limited and the search for new therapies impeded by the absence of a reliable animal model. In our work, we determined that NMOSD is characterized by decreased IFN-γ receptor signalling and that IFN-γ depletion in $AQP4_{201–220}$-immunized C57BL/6 mice results in severe clinical disease resembling human NMOSD. Pathologically, the disease causes autoimmune astrocytic and CNS injury secondary to cellular and humoral inflammation. Immunologically, the absence of IFN-γ allows for increased expression of IL-6 in B cells and activation of Th17 cells, and generation of a robust autoimmune inflammatory response. Consistent with NMOSD, the experimental disease is exacerbated by administration of IFN-β, whereas repletion of IFN-γ, as well as therapeutic targeting of IL-17A, IL-6R and B cells, ameliorates it. We also demonstrate that immune tolerization with $AQP4_{201–220}$-coupled poly(lactic-co-glycolic acid) nanoparticles could both prevent and effectively treat the disease. Our findings enhance the understanding of NMOSD pathogenesis and provide a platform for the development of immune tolerance-based therapies, avoiding the limitations of the current immunosuppressive therapies.

1 Department of Microbiology-Immunology, Feinberg School of Medicine, Northwestern University, Chicago, IL 60611, USA
2 Department of Neurology, Feinberg School of Medicine, Northwestern University, Chicago, IL 60611, USA
3 Department of Biology, Loyola University Chicago, Chicago, IL 60660, USA
4 COUR Pharmaceutical Development Company, Inc., Northbrook, IL 60077, USA

Correspondence to: Roumen Balabanov, MD
Department of Neurology
Northwestern University Feinberg School of Medicine
303 E. Chicago Avenue, Chicago, IL 60611, USA
E-mail: roumen.balabanov@nm.org

Correspondence may also be addressed to: Stephen D. Miller, PhD
Department of Microbiology-Immunology
Northwestern University Feinberg School of Medicine
7-716 Tarry Building, 303 E. Chicago Avenue, Chicago, IL 60611, USA
E-mail: s-d-miller@northwestern.edu

Keywords: neuromyelitis optica spectrum disorder; aquaporin 4; interferon-γ; animal model; immune tolerance

Received January 27, 2023. Revised September 27, 2023. Accepted October 21, 2023. Advance access publication November 1, 2023

Introduction

Neuromyelitis optica spectrum disorder (NMOSD) is an autoimmune inflammatory disease of the CNS, affecting predominantly the optic nerves and spinal cord, and to a lesser extent the brain.[1] The disease is mediated by self-reactive T helper 17 (Th17) cells and an antibody directed against the astrocytic water channel protein aquaporin 4 (AQP4).[2,3] It is believed that autoimmune inflammation arises in the peripheral immune organs and evolves in a cascade-like fashion, involving several cytokines and effector molecules, including IL-6, IL-17, the complement system, as well as mononuclear and polymorphonuclear cells.[4-9] Pathologically, the disease is a result of the convergence of the multiple effector arms of the immune system, leading to direct astrocyte injury and bystander demyelination, oligodendrocyte loss and neuronal damage.[4,8,10-12] Immunotherapy of NMOSD is founded on disease pathogenesis and targets the B cells, IL-6R and complement, but despite its immunosuppressive effect, it possesses limited potential to eradicate autoimmune clones.[13-18]

Immune tolerization is an experimental and clinical therapeutic approach of major interest to the field of NMOSD.[19] This interest is fostered by the fact that the AQP4 autoantigen targeted in the NMOSD is well characterized and that anti-AQP4 immune responses are quantifiable and correlate with disease activity. However, research on immune tolerance and other immunotherapies is impeded by the very low incidence of NMOSD, which is about 14 per 100 000 population, and the limited availability of human specimens for extensive studies.[1] Moreover, current animal models of the disease have failed to recapitulate its clinicopathological characteristics fully, in terms of immune mechanisms, natural course and clinical relevance, or they require elaborate manipulation, making them suboptimal or inaccessible for NMOSD research.[20,21]

Interferons (IFNs) play an important role in the pathogenesis of CNS-autoimmune diseases by altering and modulating the balance between the disease-specific Th1 and Th17 responses.[22-29] IFN-β (type I IFN), a common therapy for multiple sclerosis due to its inhibitory effects on Th1 cells, worsens symptoms in NMOSD.[22,23] Disease symptoms and severity positively correlate with the degree of Th17 immune dominant responses, IL-6 levels and anti-AQP4 antibody titres.[7,30-33] Alternatively, IFN-γ (type II IFN) plays a pro-inflammatory role in the pathogenesis of multiple sclerosis by stimulating Th1 responses,[24] while its role in NMOSD is uncertain, as reports have described both up- and downregulation of its expression and/or associated genes.[32,34-43] This pattern of functional opposition between type I and II IFNs is of major interest given its clinical implications for NMOSD. It is conceivable that IFN-γ might be involved in the pathogenesis of the disease as a negative regulator of autoreactive immune responses and CNS inflammation.

In the present report, we describe the role of IFN-γ in NMOSD and $AQP4_{201–220}$-induced experimental disease. Our study demonstrates for the first time that IFN-γ is essential for maintaining natural immune tolerance to AQP4 and that its absence allows the generation of a significant autoimmune inflammation, and a severe clinical disease resembling NMOSD. The results of this study are novel and provide an experimental paradigm for testing new therapies for NMOSD.

Materials and methods

Induction of $AQP4_{201–220}$ disease

Male or female C57BL/6 wild-type (WT), IFN-γ-receptor-knockout (IFNGRKO),[44] IFN-γ-knockout (IFNGKO),[45] type I IFN-receptor-knockout (IFNARKO),[46] FoxP3 diptheria toxin receptor ($FOXP3^{DTR}$)[47] and IghelMD4[48] mice 8–12 weeks old were purchased from the Jackson Laboratories. AQP4 knockout (AQP4KO) mice[49] were acquired from Riken BRC, Japan. Mice were immunized with the immunodominant AQP4 peptide 201–220 ($AQP4_{201–220}$; Genemed Synthesis)[50] using various concentrations of the peptide. Complete Freund's adjuvant (CFA) and pertussis toxin (PTx) administration was as previously described (Supplementary Fig. 1).[51,52] Disease signs were scored as follows: 0 = no symptoms; 1 = loss of tail tone; 2 = flaccid tail; 3 = partial paralysis of lower extremities; 4 = complete paralysis of lower extremities; 5 = moribund/death.

Mouse treatments

Treatment antibodies/isotype controls (BioXcell) were administered intraperitoneally (i.p.) in 200 µl/PBS at predetermined days post-immunization (p.i.): anti-IFN-γ (500 µg, clone XMG1.2) at Days 0, 7, 14 and 21; anti-IL-6R (1 mg, clone 15A7) at Days 0 and 7; anti-CD20 (200 mg, clone MB20–11) at Days 0, 7 and 14; anti-CD25 (500 mg, clone PC-61.5.3) at Days 0 and 2; anti-IL-17A (500 mg, clone 17F3) weekly from Day 0 or at Days 6, 10 and 14; and mouse IFN-γ (2 µg; Gibco) or IFN-β (10 000 U; BioLegend) from Day 0 for 10 days or at the peak of the disease daily for 7 days. $AQP4_{201–220}$-coupled or $OVA_{323–339}$-coupled poly(lactic-co-glycolic acid) (PLGA) nanoparticles (1.28 mg/200 µl) were given intravenously (i.v.)-one injection at Day 7 prior to immunization or two therapeutic injections at symptom onset. T regulatory cell (T_{reg}) depletion in $FOXP3^{DTR}$-mice was induced by administering 2.5 µg of diphtheria toxin (DTx; Sigma-Aldrich) at Days 8 and 10.

Immunofluorescence

Optic nerves, spinal cord and brain were fixed and processed as previously described.[53] Primary antibodies included: rabbit anti-AQP4 (1:200; Sigma), rabbit anti-Sox9 (1:500; Invitrogen), mouse anti-Sox9 (1:500; Novus), chicken anti-GFAP (1:200; Millipore) chicken anti-neurofilament (1:500; Millipore), rat anti-CD3 (1:200; Santa Cruz), rat anti-MBP (1:250; Bio-Rad), mouse anti-CD19 (1:50; ThermoFisher), mouse anti-C5b-9 (1:50; Santa Cruz), goat anti-mouse IgG (heavy + light) (1:2000; Invitrogen) and goat anti-TPPP (1:100; ThermoFisher). The nuclei were counterstained with DAPI. Images were acquired and analysed using a fluorescent confocal microscope (Zeiss-LSD 880) (Supplementary material).

Flow cytometry

Single-cell suspensions of CNS-mononuclear cells, lymph nodes and spleens were obtained as previously described.[51,54,55] Flow cytometry cell analysis was performed using a FACSCelesta™ (BD Bioscience) and analysed with FlowJo X v10.7 software (Tree Star).[52] T-cell cytokine expression was assessed following stimulation with phorbol myristate acetate (PMA)/ionomycin (BioLegend) and Brefeldin A (BD Bioscience). The immunostaining used in the experiments consisted of the following immunophenotyping panels. White blood cells: CD45, CD3, CD19, NK1.1, CD11b, F4/80 and Ly6G; T cells: CD45, CD3, CD4, γδTCR, IL-17A, IFN-γ; B cells: CD19, CD138, CD40, CD80, CD86, MHC-II, IL-6; Th17-cell differentiation: CD4, IL-17A, granulocyte-macrophage colony-stimulating factor (GM-CSF), CD25, RAR-related receptor-gamma (RORγt), FOXP3; astrocytes: GLAST, AQP4, CD45 (Supplementary Fig. 2 and Supplementary material).

RNA analysis

Data for differentially expressed genes (DEGs) from whole blood of NMOSD patients versus healthy controls were obtained from

publicly accessible data published by Agasing *et al.*[7] The Interferome database[56] was used to determine type I or type II IFN-regulated genes. Reactome software[57] analysis was performed to obtain the most significant enriched pathways. Mouse total RNA was analysed with a Nanostring® autoimmune profiling panel. Rosalind® software was used to complete mRNA DEG analysis. Gene set analysis (GSA) was performed with a fold-change of 1.5 for up- and downregulated genes and adjusted *P*-value of 0.05.

In vitro B-cell stimulation and Th17 induction

B cells were purified using negative magnetic selection (Stemcell Technologies), cultured at 2.5×10^6 cells/ml and stimulated for 24 or 72 h with 40 μg/ml $AQP4_{201–220}$ peptide or 1 μg/ml of plate bound anti-CD40 antibody. WT and IFNGKO B cells were also stimulated with 0, 1, 25 and 100 ng/ml of IFN-γ. For Th17 induction, B cells were stimulated with either $AQP4_{201–202}$ or anti-CD40 antibody for 24 h and replated in the presence of 20 μg/ml $AQP4_{201–220}$ together with purified $CD4^+$ cells from primed IFNGRKO mice (2.5×10^6 cells/ml) in a 1:1 ratio for 72 h. Cells were analysed by flow cytometry and multiplex cytokine assay.

Multiplex cytokine and anti-AQP4 ELISAs

Splenocyte *ex vivo* recall assays were performed by culturing cells at 37°C with 20, 40 and 80 μg/ml of $AQP4_{201–220}$ peptide or 1 μg/ml of anti-CD3 antibody for 72 h. The Multiplex cytokine assay and Luminex® 200™ system were used to quantitate cytokines IL-1β, IL-4, IL-6, IL-10, IL-17A, IL-23, GM-CSF, IFN-γ and TNF-α. These cytokines plus chemokines CXCL1, CXCL2, CXCL9, CCL2, CCL3, CCL4 and CCL5 were also quantitated in mouse sera (Millipore). Serum $AQP4_{201–220}$-specific antibodies were quantitated using ELISAs. A 96-well high-binding plate (Fischer Scientific) was coated with 1 μg/ml of $AQP4_{201–220}$ or recombinant human AQP4 protein (provided by Dr Robert Stroud, UCSF), and mouse serum was added to a final dilution of 1:50. Horseradish peroxidase-labelled detection antibodies (1:4000) and tetramethylbenzidine substrate (SurModics) were used to develop the plates, and the product's optical density (OD) was measured on a SpectraMax-M2 plate reader. The immunoreactivity of anti-AQP4 IgG was also tested in a cell-based assay (Supplementary material).

Statistical analyses

Statistical analyses were performed using the Mann–Whitney non-parametric test or Kruskal–Wallis one-way ANOVA with GraphPad Prism v.9.5 software. Differences with *P*-values of ≤ 0.05 were considered significant.

Results

IFN-γ-dependent genes are differentially expressed in NMOSD

To investigate the roles of type I (IFN-β) and II (IFN-γ) IFNs in NMOSD, we analysed the 87 DEGs previously identified in whole blood of untreated NMOSD patients versus healthy controls.[7] Using the Interferome database, we identified 69/87 DEGs strictly regulated by IFNs (Fig. 1A). DEGs controlled by only type I or type II IFNs were predominantly downregulated (2/2 and 13/14 genes, respectively), whereas those controlled by both IFNs were mostly upregulated (41/53 genes). Biologically, the 16 DEGs controlled by only type I or type II IFNs appeared to be pleiotropic in their function. Alternatively, DEGs regulated by both IFNs displayed more uniform and recognizable patterns, such as IFN-inducible, anti-viral and immune response-related genes. Analysis using the Reactome software of the 87 DEGs demonstrated that the most common signalling pathways associated with NMOSD were those of IFN, IFN-α/β, IFN-γ, cytokine and antiviral responses (Fig. 1B). Most of the DEGs associated with NMOSD (67/87) were either strictly dependent or co-dependent on IFN-γ receptor signalling.

Absence of IFN-γ signalling enhances $AQP4_{201–220}$-induced disease

As previously reported, immunization of C57BL/6 mice with an immunodominant $AQP4_{201–220}$ peptide emulsified in CFA, although effective in inducing an autoimmune response, was insufficient to induce robust inflammation and a paralytic experimental disease.[50] We attempted, first, to increase the disease severity to a clinically relevant level using common experimental strategies. Our results revealed that immunization with higher concentrations of $AQP4_{201–220}$ peptide (200 μg) and CFA [500 μg of *Mycobacterium tuberculosis* (Mtb)] than previously employed yielded only minimal enhancement of symptoms (Supplementary Fig. 1 and Supplementary Table 1). Similarly, T_{reg} cell blockade/depletion using anti-CD25 neutralizing antibodies in WT and DTx-induced depletion in $FOXP3^{DTR}$ mice failed to increase disease incidence and severity significantly (Supplementary Fig. 3).[58]

Next, we immunized WT, IFNARKO, IFNGRKO and IFNGKO mice with $AQP4_{201–220}$ peptide as specified above. IFNARKO mice exhibited a low incidence (40%) and mean clinical score (MCS = 1.0), lower than WT mice (67% incidence, MCS = 1.77). Significantly more severe disease was seen in mice lacking either IFN-γ or its receptor (IFNGKO: 80% incidence, MCS = 3.1; IFNGRKO: 80% incidence, MCS = 3.3) (Fig. 1C and D and Supplementary Video 1). These mice exhibited a slightly delayed mean day of onset (MDO) of 17.8 and 20.8, respectively, compared with the WT and IFNARKO mice (MDO = 13.6 and 17, respectively) (Supplementary Table 2A). However, their disease was severe and persisted chronically without remission compared with the WT and IFNARKO mice (Fig. 1C). The effect of anti-IFN-γ neutralization in $AQP4_{201–220}$-immunized WT mice was dose-dependent. While no clinical effects were observed following the administration of two doses, a slight enhancement of the disease was noted after three doses, and significantly more severe outcomes were observed with four doses, amongst increased disease incidence (20%, 40% and 90%, respectively) and MCS (0.55, 1.15, and 3.65, respectively) (Fig. 1E and F and Supplementary Table 2B). The number of doses also determined the disease chronicity and recovery (improvement ≥1 score), as mice developing disease after two or three doses of anti-IFN-γ recovered over time (100% and 50% recovery rate per dose, respectively) compared with the group that received four doses (11% recovery). Thus, IFN-γ controls the clinical course of $AQP4_{201–220}$-induced disease, and its depletion/neutralization is required for the induction of clinically relevant symptomology.

Opposing roles of type I and type II IFNs in $AQP4_{201–220}$-induced disease

To determine the differential roles of type I and type II IFNs on disease modulation, we treated IFNARKO or IFNGRKO mice for 10 days with IFN-γ and IFN-β, respectively. Although WT mice developed a mild/low severity disease, IFN-γ treatment of WT mice still reduced the incidence (30% to 20%) and maximal MCS (0.8–0.25) and delayed the MDO (from Day 13 to Day 17) compared with the controls (Fig. 1G and Supplementary Table 2C). This treatment had no effect on IFNARKO mice (Fig. 1H). In WT mice, IFN-β treatment displayed

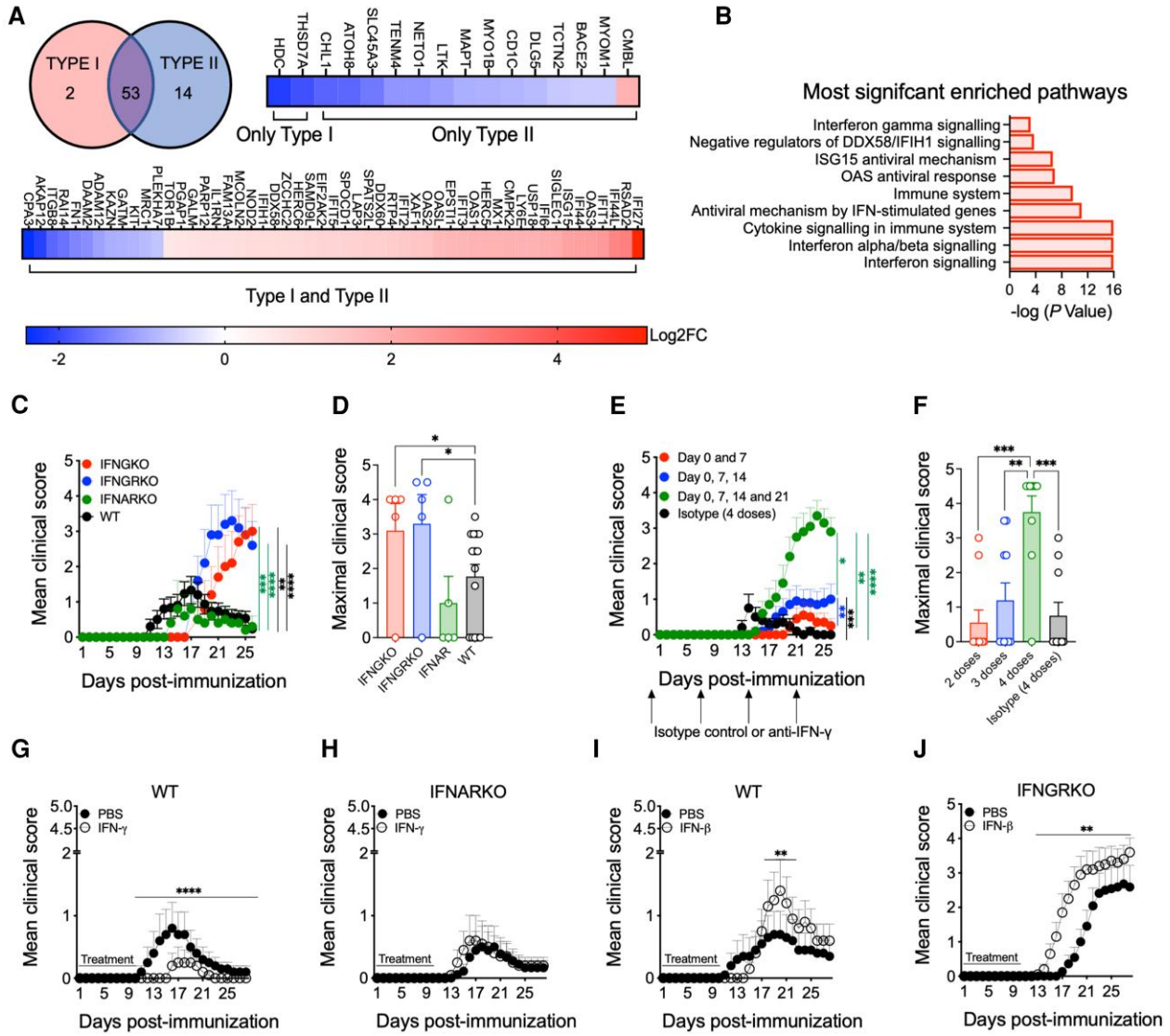

Figure 1 Opposing roles of type I and type II interferons in the regulation of neuromyelitis optica spectrum disorder and AQP4$_{201–220}$-induced disease. (**A**) Venn diagram and differentially expressed genes (DEGs) following Interferome analysis for type I and type II IFN-regulated genes (a total of 69 of 87 genes regulated by IFNs) from whole blood of untreated neuromyelitis optica spectrum disorder (NMOSD) patients versus healthy donors obtained from publicly available RNA sequencing data (see 'Materials and methods' section). (**B**) Reactome pathway enrichment analysis of DEGs (total of 87 DEGs). Mean clinical score (**C**) and maximal clinical score (**D**) were evaluated in AQP4$_{201–220}$-immunized wild-type (WT) (black, $n = 15$), IFN-γ-knockout (IFNGKO; red, $n = 5$), IFN-γ-receptor knockout (IFNGRKO; blue, $n = 5$) and type I IFN-receptor knockout (IFNARKO; green, $n = 5$) mice. Mean clinical scores (**E**) and maximal clinical scores (**F**) were recorded in AQP4$_{201–220}$-immunized WT mice treated with two (red, $n = 10$), 3 (blue, $n = 10$) or four (green, $n = 10$) weekly doses starting from Day 0 of anti-IFN-γ, or isotype control antibodies (filled circles, total of four doses, $n = 10$). Administration of IFN-γ to WT (**G**) and IFNARKO (**H**), or IFN-β to WT (**I**) and IFNGRKO (**J**) mice was performed for 10 days beginning on the day of immunization ($n = 10$). All data are presented as mean ± standard error of the mean (SEM). Statistical analyses were performed using the Mann–Whitney test. $^*P < 0.05$, $^{**}P < 0.01$, $^{***}P < 0.001$.

the opposite effects, increasing disease incidence (30% to 50%) and the maximal MCS (0.7 to 1.4), while the MDO was moderately delayed (from Day 14 to Day 16) (Fig. 1I and Supplementary Table 2D). The treatment led to significantly more severe disease in IFNGRKO mice, with higher incidence (63% to 90%), maximal MCS (2.682 to 3.6) and earlier MDO (from Day 19 to Day 16) (Fig. 1J and Supplementary Table 2D).

AQP4$_{201–220}$-induced disease is characterized by specific astrocytic and bystander CNS cell injury

Pathological examination of anti-IFN-γ-treated mice at Day 22 p.i. demonstrated a significantly reduced number of cells expressing SOX9 (astrocyte-specific nuclear transcription factor)[59] in the spinal cord (51% reduction) and AQP4 loss in optic nerve and spinal cord (49% and 48%, respectively) compared with the controls, indicating the antigen and cell specificity of the autoimmune response. GFAP staining revealed a morphology of reactive astrocytes in both structures (Fig. 2A and B).[60] Flow cytometry analysis further demonstrated that GLAST (EAAT1), another astrocyte marker, was also reduced in the spinal cord of anti-IFN-γ-treated mice (47% reduction), indicating inflammatory cell injury (Supplementary Fig. 4).[61] Additionally, we noticed in the optic nerves and spinal cord, significant bystander loss of myelin [38.7% reduction in MBP mean fluorescence intensity (MFI) and 5.3-fold increase in demyelination area, respectively],

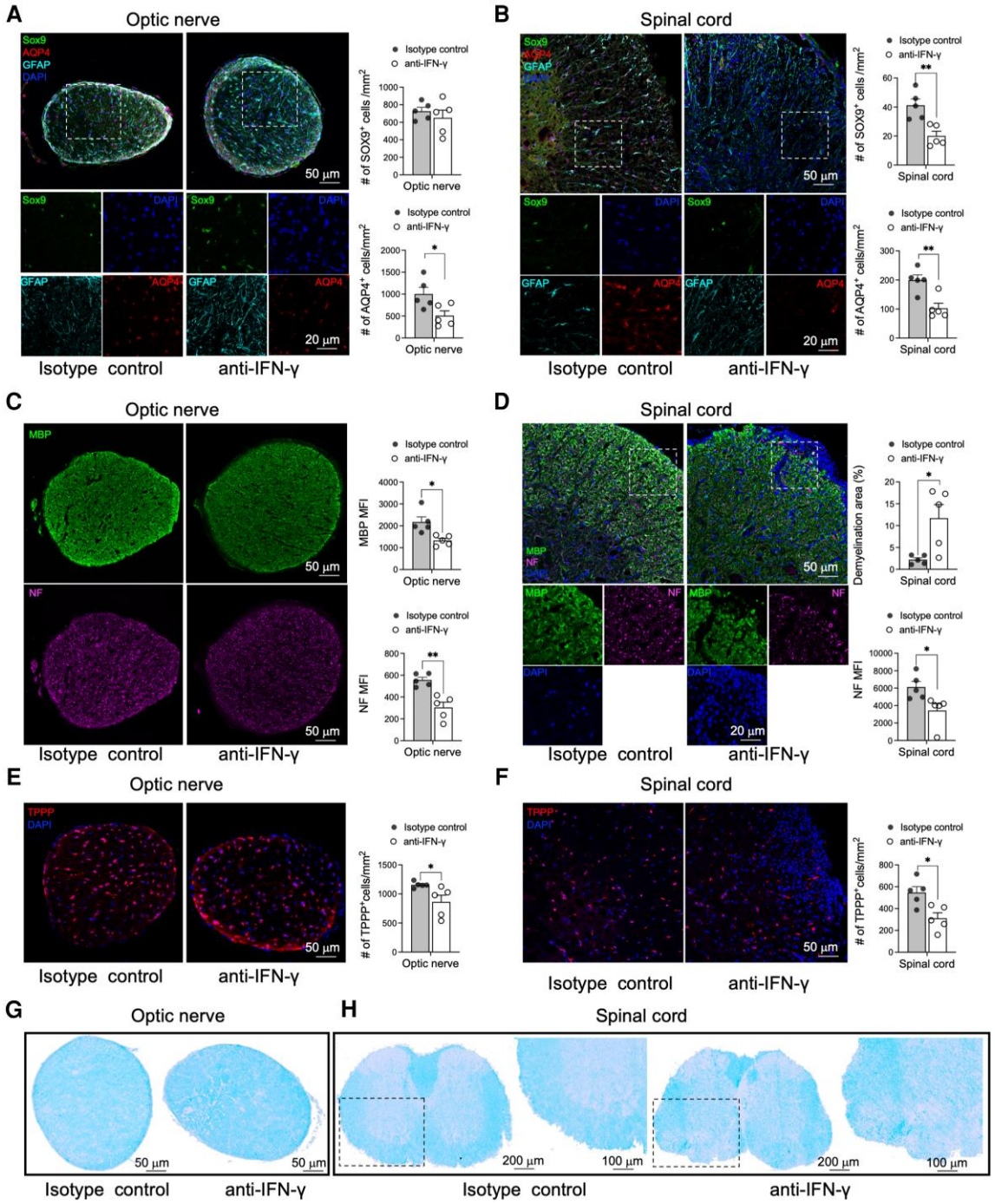

Figure 2 AQP4$_{201–220}$-induced disease is characterized by loss of astrocytes, oligodendrocytes, myelin and axons. Optic nerve (**A**, **C** and **E**) and lumbar spinal cord (**B**, **D** and **F**) sections were obtained from isotype control- and anti-IFN-γ-treated mice at Day 22 post-immunization (p.i.) and immunostained for astrocyte (Sox9-AQP4-GFAP-DAPI) (**A** and **B**), myelin (MBP-DAPI), neurofilament (NF-DAPI) (**C** and **D**) and oligodendrocyte (TPPP-DAPI) markers (**E** and **F**). The immunofluorescent images were accompanied by a statistical comparison of the markers' mean fluorescence intensity (MFI) between the isotype control- and anti-IFN-γ-treated groups. Luxol fast blue (LFB) staining was performed to examine optic nerve (**G**) and lumbar spinal cord (**H**) for evidence of demyelination. The rectangle delineates an area of the anterior spinal columns that demonstrates loss of LFB staining depicted at low and high magnifications. Scale bars of 20, 50, 100 and 200 μm are indicated on the images. All data are presented as mean ± SEM ($n = 5$). Statistical analyses were performed using the Mann–Whitney test. $^{*}P < 0.05$, $^{**}P < 0.01$.

oligodendrocytes (25% and 43.1% TPPP^{+} cell reduction, respectively) and neurofilaments/axons (45.15% and 43.9% NF MFI reduction, respectively) was observed (Fig. 2C–F and Supplementary Fig. 5). Myelin loss was independently confirmed by using Luxol fast blue (LFB) staining (Fig. 2G and H).

IFN-γ regulates immune responses in AQP4$_{201–220}$-induced disease

Immunopathological examination of AQP4$_{201–220}$-induced disease demonstrated that optic nerve and spinal cords of anti-IFN-γ-treated WT

mice were significantly more inflamed and infiltrated with $CD3^+$ T cells and $CD19^+$ B cells compared with the isotype control group (Fig. 3A–D). The T cells appeared to be localized within the tissue parenchyma, whereas the B cells were distributed predominantly along the meninges. IFN-γ-depleted mice also displayed deposits of C5b, indicating activation of the complement system, which colocalized with IgG (Fig. 3E and F). CD3, CD19, C5b and IgG staining was also observed in brains of the anti-IFN-γ-treated group (Supplementary Fig. 6). Anti-$AQP4_{201–220}$ antibodies were detected in both anti-IFN-γ antibody- and isotype control-treated mice following immunization. Autoantibody levels in both groups displayed comparable levels and patterns of isotype class-switching, with a rise and subsequent decrease in anti-$AQP4_{201–220}$ IgM, followed by a significant increase in anti-$AQP4_{201–220}$ IgG levels, from Days 14 to 28 p.i. (Fig. 3G). There was significantly less IgG in the anti-IFN-γ-treated group on Day 14 [OD (mean) = 1.409] versus the isotype control group [OD (mean) = 2.364], correlating with the delayed disease onset observed. This difference was transient and at Day 28 p.i. both groups demonstrated similar levels of anti-$AQP4_{201–220}$ IgG levels [OD (mean) = 3.171 versus 3.490 for anti-IFN-γ-treated and control groups, respectively]. We detected an IgG response against the full recombinant human AQP4 (rhAQP4) protein, which was enhanced in the anti-IFN-γ-treated group at Day 28 p.i. compared with the controls [OD (mean) = 0.592 versus 0.32, respectively] (Fig. 3H). The presence of this anti-AQP4 IgG was confirmed independently by showing post-immunization serum, collected from either anti-IFN-γ-treated WT or IFNGRKO mice, stained live CNS cells isolated from WT (1.3- and 1.5-fold-increase in IgG^+ anti-AQP4, respectively compared with pre-immunization controls) but not from AQP4KO mice (Supplementary Fig. 7).

We also analysed the serum levels of various cytokines and chemokines during the disease course. Comparatively, only IL-17A levels were significantly elevated with anti-IFN-γ treatment, with a peak at Day 14 p.i., 4-fold increase compared with isotype controls, indicating that depletion of IFN-γ favours a Th17 immune bias (Fig. 3I).[2,35,37,62] Levels of IL-6[32,63] were increased at Day 14 p.i. in both groups but higher in the anti-IFN-γ-treated group (1.8-fold increase). Interestingly, serum IFN-γ levels were significantly higher at Day 28 p.i. in the anti-IFN-γ-treated group (2.42-fold increase) (Supplementary Fig. 8A). We also observed a significant increase of the neutrophil chemoattractants CCL3 at Day 14 p.i. (2.14-fold increase) and CXCL2 at Day 28 p.i. (3.08-fold increase) (Fig. 3J). Monocyte and macrophage chemoattractants CCL2 (1.83-fold increase) and CCL4 (12.2-fold increase) were also significantly elevated at Day 28 p.i. compared with the control group (Supplementary Fig. 8B). *Ex vivo* recall analysis of splenic cells stimulated with $AQP4_{201–220}$ or anti-CD3 at Day 18 p.i. demonstrated significantly elevated levels of secreted GM-CSF, IL-6 and IL-1β (fold increases of 1.72, 2.09 and 1.82, respectively) (Fig. 3K and L and Supplementary Fig. 8C), while anti-CD3 stimulation only displayed a significant decrease in IL-4 secretion (73% reduction).

IFN-γ controls Th17-driven CNS inflammation in $AQP4_{201–220}$-induced disease

We next isolated mononuclear cells from the spinal cord of anti-IFN-γ- and isotype control-treated groups at Day 22 p.i. and performed flow cytometry and mRNA expression analyses (Fig. 4A). Globally, the total number of isolated cells (2.65-fold increase) and $CD45^+$ immune cells (5.77-fold increase) were significantly more abundant in the anti-IFN-γ-treated group than in the control group (Fig. 4B). A microarray analysis of 750 genes associated with autoimmune responses was performed, identifying a total of 18 DEGs, 6/18 upregulated and 12/18 downregulated (Fig. 4C). Some of the upregulated genes were directly related to the Th17-signalling pathway (*Il17a*, *Rorc*, *Cd4* and *I1r1*), which is consistent with our earlier observations of increased serum levels of IL-17 and expression of IL-1β by splenic T cells in the *ex vivo* recall experiments (Fig. 3I and Supplementary Fig. 8C). MHC class II (MHC-II) DEGs were downregulated (*H2-eb1*, *H2-aa* and *Cd74*) as well as the regulatory cytokine IL-10 DEGs.[64] Significantly, GSA examination indicated that upregulation of Th17 differentiation and complement system genes are the two principal processes associated with the experimental disease, while MHC gene expression was found to be downregulated (Fig. 4D and E). Simultaneous analysis performed on the spleen cells from the same groups showed a total of 30 DEGs (20 upregulated and 10 downregulated). Notably, Th17-mediated processes and B-cell receptor signalling were significantly upregulated (Supplementary Fig. 9). In the spleen, the IL-6Rβ gene (*Il6st*) was also upregulated, whereas the complement system genes were downregulated. The latter finding may indicate that local complement secretion and deposition (Fig. 3E and F) by mononuclear cells occurs mainly within the CNS.[65]

Although resident non-activated microglia ($CD45^{lo}CD11b^+$) numbers did not change, there was a significant reduction in their frequency (64% reduced), indicating higher activation of this population in diseased anti-IFN-γ-treated mice (Fig. 4B).[51] This correlates with a higher number and frequency of activated macrophages/microglia ($CD45^{hi}CD11b^+$) (6.6- and 2.1-fold increases, respectively) and $F4/80^+$ macrophages/microglia (8.58- and 2.7-fold increases, respectively) (Fig. 4F). Significant increases in the numbers of neutrophils, B cells, NK cells and T cells were also observed (4.43-, 3.57-, 2.2- and 9.52-fold increases, respectively) (Fig. 4G and H). Total $CD4^+$, $CD4^+IL\text{-}17A^+$, $\gamma\delta TCR^+$ and $\gamma\delta TCR^+IL\text{-}17A^+$ cell numbers were significantly increased (4.53-, 4.52-, 3.65- and 5.96-fold increases, respectively) in the CNS of the anti-IFN-γ-treated group (Fig. 4I and J). Only the frequency of total $CD4^+$ cells (2.1-fold increase) was significantly upregulated, while the frequency of IL-17A was significantly higher in both $CD4^+$ (2.08-fold increase) and $\gamma\delta TCR^+$ T cells (2.71-fold increase) (Fig. 4I and J and Supplementary Fig. 10A). The frequencies of IFN-γ $CD4^+$ and γδTCR T cells were also significantly higher in the spinal cord (4.7- and 4.1-fold increases, respectively). Similar infiltration patterns were also detected in the brain (Supplementary Fig. 10B–D). In the secondary immune organs, the absence of IFN-γ was associated with significantly increased frequencies of $CD4^+IL\text{-}17A^+$ and $\gamma\delta TCR^+IFN\text{-}\gamma^+$ T cells (1.44- and 1.26-fold increases, respectively) in lymph nodes and reduced B-cell numbers (30% reduction) in the spleen (Supplementary Figs 9E and 10E). To confirm the pathogenic role of IL-17A, we treated IFNGRKO mice weekly (Fig. 4K) or with three doses (Fig. 4L) spanning the peak of serum IL-17A (Fig. 3I). Neutralization of anti-IL-17A led to a significantly lower disease incidence (weekly treatment: 42% versus 66%; three doses: 66% versus 100%) and severity (weekly treatment: MCS 1.21 versus 2.83; three doses: MCS 1.58 versus 4.17) compared with the isotype control-treated mice.

Lastly, treatment of IFNGKO mice with recombinant IFN-γ for 7 days, starting at the peak of the disease, rapidly suppressed disease progression with a sustained reduction of clinical symptoms compared with PBS-treated controls (pretreatment MCS: 2.92 and 3.07; post-treatment MCS: 2.5 and 3.92; for the IFN-γ and PBS groups, respectively) (Fig. 5A). Notably, once the treatment was discontinued, IFN-γ-treated mice relapsed to an MCS of 3.38 (Supplementary Fig. 11A), indicating, together with the dose-dependent enhanced clinical responses upon anti-IFN-γ

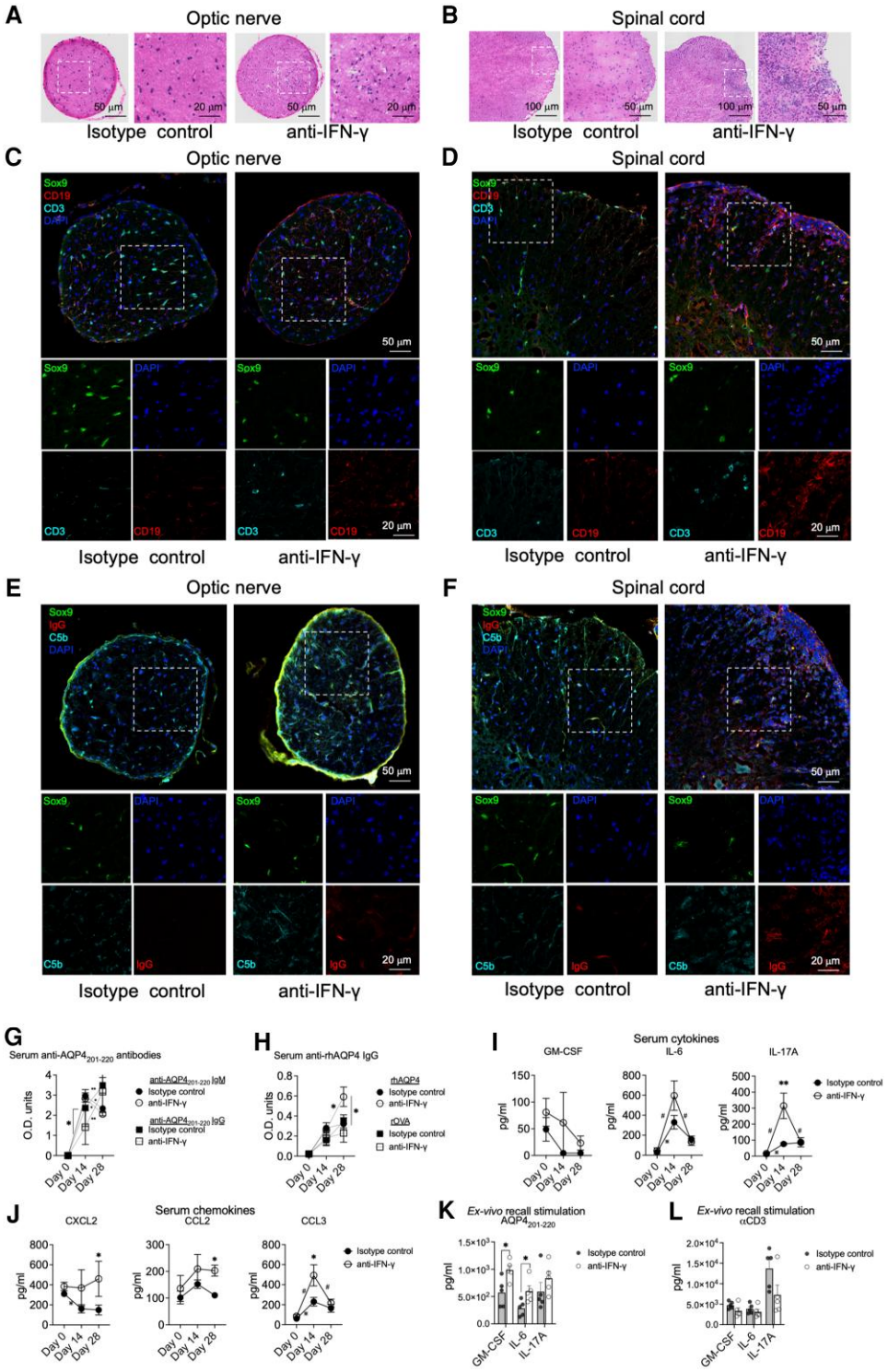

Figure 3 IFN-γ regulates peripheral immune responses and CNS infiltration of inflammatory cells in AQP4$_{201–220}$-induced disease. Optic nerve (**A**, **C** and **E**) and spinal cord (**B**, **D** and **F**) sections from wild-type (WT) mice treated with either anti-IFN-γ or isotype control antibodies were analysed at Day 22 post-immunization (p.i.) using haematoxylin and eosin staining (**A** and **B**), and Sox9-CD3-CD19-DAPI (**C** and **D**), Sox9-C5b-IgG-DAPI (**E** and **F**) immunostaining. Scale bars for 20, 50 and 100 μm are indicated on the images. Optical densities of total serum levels of anti-AQP4$_{201–220}$-specific IgM (circles) and IgG (squares) in peptide-immunized mice treated with anti-IFN-γ (open circles, $n = 9$) or isotype control (filled circles, $n = 11$) antibodies were determined by ELISA before immunization at Day 0 and at Days 14 and 28 p.i. (**G**). Serum IgG antibody levels against recombinant human AQP4 (rhAQP4) or rOVA (control protein) were also determined (**H**). Serum levels of GM-CSF, IL-6 and IL-17 cytokines (**I**), and CXCL2, CCL2 and CCL3 chemokines (**J**) from AQP4$_{201–220}$-immunized mice treated with anti-IFN-γ ($n = 6$) or isotype control ($n = 6$) antibodies were determined by multiplex cytokine assay prior immunization at Day 0 and at Days 14 and 28 p.i. *Ex vivo* recall analysis was performed using supernatants (multiplex cytokine analysis of GM-CSF, IL-6 and IL-17A) from splenocytes of anti-IFN-γ-treated ($n = 5$) or isotype control-treated ($n = 5$) groups obtained at Day 18 p.i. and following cell culture for 72 h in the presence of 40 μg/ml AQP4$_{201–220}$ peptide (**K**) or 1 μg/ml of soluble anti-CD3 antibody (**L**). All data are presented as mean ± SEM. Statistical analyses were performed using the Mann–Whitney test: $^{*}P < 0.05$, $^{**}P < 0.01$; $^{\#,*}$statistically significant difference between Days 0–14 or 14–28 p.i. in anti-IFN-γ- or isotype control-treated groups, respectively.

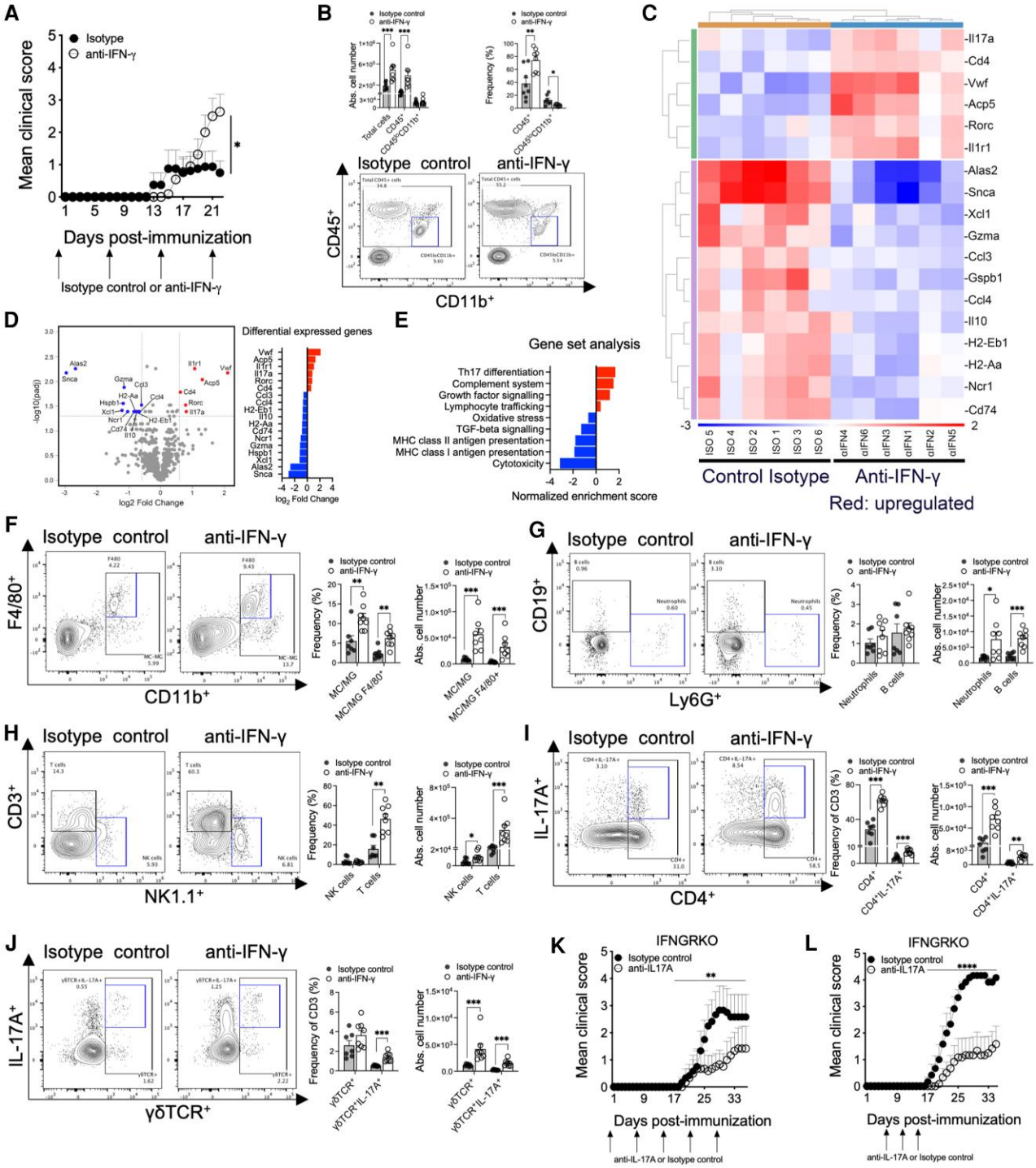

Figure 4 Anti-IFN-γ enhancement of AQP4$_{201–220}$-induced disease is driven by Th17 cells. Mean clinical scores of AQP4$_{201–220}$-immunized wild-type (WT) mice treated with anti-IFN-γ (four doses, open circles, $n = 8$) or isotype control (four doses, filled circles, $n = 11$) until Day 22 post-immunization (p.i.) (**A**). Absolute cell number of mononuclear cells obtained from the spinal cords of anti-IFN-γ-treated ($n = 8$) and isotype control-treated ($n = 7$) groups (**B**). CD45$^+$ and CD45^{lo}CD11b$^+$ cell number and frequency were analysed by flow cytometry. Total RNA from mononuclear cells obtained from the spinal cord of anti-IFN-γ-treated ($n = 6$) and isotype control-treated ($n = 6$) groups were analysed, and a hierarchical heatmap clustering was created based on the most differentially expressed genes (**C**). A Volcano plot of RNA profiles comparing anti-IFN-γ versus isotype control treatments, and pathway enrichment analysis of the most differentially expressed gene sets (**D** and **E**). Absolute cell number and frequencies of monocytes/macrophages (MC)/activated microglia (MG; CD45^{hi}), MC/MG F4/80$^+$, Neutrophils Ly6G$^+$, NK (NK1.1$^+$), CD3$^+$, CD4$^+$, CD4$^+$17A$^+$, γδTCR$^+$, γδTCR$^+$IL-17A$^+$, CD19$^+$ cells were determined by flow cytometry analyses (**F–J**). Administration of anti-IL-17A (open circles) or isotype control (filled circles) antibodies to IFNGRKO mice, as weekly doses beginning at Day 0 (**K**) or three doses beginning at Days 6, 10 and 14 p.i. ($n = 6$) (**L**). All data are presented as mean ± SEM. Statistical analyses were performed using the Mann–Whitney test. $^*P < 0.05$, $^{**}P < 0.01^{**}$ and $^{***}P < 0.001$.

treatment of WT mice (Fig. 1E), that disease chronicity and relapses are regulated by IFN-γ. Clinical improvement was associated with significantly reduced numbers of mononuclear cells (70% reduction), CD45$^+$ cells (74.8% reduction), macrophages/microglia (80% reduction), F4/80$^+$ macrophages/microglia (87.2% reduction), CD3$^+$ T cells (78.3% reduction), CD4$^+$ T cells (53.8% reduction) and a trend toward Th17 reduction (44% reduction; $P = 0.0823$) in the spinal cords compared with the controls (Fig. 5A–C). Administration of IFN-γ also significantly decreased the CD4$^+$ frequencies in the spinal cord and spleen (8% and 13.5% reduction, respectively) but without numeric population changes in spleen (Supplementary Fig. 11B). Overall, IFN-γ can inhibit clinical symptoms of AQP4$_{201–220}$-induced disease through suppression of the CNS-inflammation and by modulation of pathogenic Th17 cell response.[7,30-32]

AQP4$_{201–220}$-induced disease is strictly dependent on B-cell activation

As GSA showed significantly upregulated B-cell receptor signalling in anti-IFN-γ-treated mice (Supplementary Fig. 9C), we examined the involvement of B cells in the experimental disease. We first tested if IFN-γ affected the expression of B-cell activation markers (IL-6, CD40, CD80, CD86 and MHC-II). Notably, at Day 22 p.i., only IL-6 expression by CD19$^+$ cells was significantly greater in terms of cell frequency (1.77-fold increase) and expression level (6.91-fold increase in MFI) in the spleens of IFNGKO compared with WT mice, corresponding with increased *il6st* DEG expression in anti-IFN-γ-treated mice (Fig. 5D and Supplementary Fig. 11C). No significant differences in the expression of the other Th17-driving cytokines, IL-1β and IL-23, was observed (Supplementary Fig. 11D). CD19$^+$ cells from IFNGKO also expressed less CD40 (30% reduction) compared with the WT group at Day 10 p.i. (Fig. 5D). The *in vitro* expression of IL-6 by purified splenic IFNGKO-B cells (Day 22 p.i.) was found to be upregulated following stimulation with either AQP4$_{201–220}$ and plate-bound anti-CD40 antibody for 72 h compared with WT B cells. Importantly, adding 25 and 100 ng/ml of IFN-γ to the cultures had suppressive effects on IL-6 production (80% and 73% reduction, respectively) only upon B-cell stimulation with AQP4$_{201–220}$ but not upon non-specific anti-CD40 stimulation (Fig. 5E and Supplementary Fig. 11E). These results demonstrate a direct regulatory role of IFN-γ in the activation of pathogenic AQP4$_{201–220}$-B cells.

Treatment with anti-CD20 antibody on Days 0, 7 and 14 p.i. significantly ameliorated the incidence of the disease in IFNGRKO mice (31% anti-CD20-treated versus 92% isotype control) and the MCS (2.3 versus 3.14) (Fig. 6A). B-cell depletion significantly lowered the serum anti-AQP4$_{201–220}$ IgM antibody levels at Day 14 p.i. [OD (mean) = 1.305 versus 2.384 for anti-CD20-treated and control groups, respectively] and at 28 p.i. [OD (mean) = 0.513 versus 1.421], as well as the anti-AQP4$_{201–220}$ IgG levels at Day 28 p.i. [OD (mean) = 1.725 versus 2.979 for anti-CD20-treated and control groups, respectively] (Fig. 6B). Anti-CD20 treatment also significantly decreased *ex vivo* spleen recall production of IL-17A (75.9% reduction) and GM-CSF (65.5% reduction) (Fig. 6C). It also significantly reduced the numbers of infiltrating mononuclear cells (62% reduction), total CD45$^+$ cells (64.5% reduction), CD4$^+$ T cells (51.1% reduction) and CD4$^+$GM-CSF$^+$ T cells (62.1% reduction) in the CNS, with significantly decreased numbers of CD4$^+$IL-17A$^+$ T cells in the spleen (44.1% reduction) at Day 28 p.i. (Fig. 6D and E). Lastly, we demonstrated that AQP4$_{201–220}$ immunization of anti-IFN-γ-treated IghelMD4 mice, in which the B cell receptor is specific for a hen egg white lysozyme, completely failed to induce clinical disease and production of anti-AQP4$_{201–220}$ IgG. Remarkably, the *ex vivo* splenic recall to AQP4$_{201–220}$ displayed dramatically lower levels of GM-CSF and IL-6 (90 and 88% less secretion, respectively), while remaining fully responsive to non-specific stimulation with anti-CD3 antibody, with an upregulation of IL-17A (Fig. 6F–H). Thus, B cells and their activation are strictly required for the initiation of AQP4$_{201–220}$-induced disease and Th17 bias, both directly modulated by IFN-γ.

IL-6 signalling modulates B-cell and Th17-cell activation and differentiation

Treatment with anti-IL-6R antibody on Days 0 and 7 p.i. led to a statistically significant reduction of disease severity and incidence in IFNGRKO mice (from 75% to 50%) and to a decrease in CD4$^+$ cell frequency in the CNS (21% reduction, Day 28 p.i.) (Fig. 7A and Supplementary Fig. 12A). The levels of anti-AQP4$_{201–220}$ IgM and IgG were like the isotype controls, despite a trend towards lowered IgM levels at Day 14 p.i. (Fig. 7B). Analysis of antibody-secreting cells at Day 8 p.i., after the second dose of anti-IL-6R, showed a significantly reduced frequency of splenic CD19$^+$CD138$^+$ plasma cells in anti-IL-6R- versus control-treated mice (36% reduction) (Fig. 7C), with no significant changes in the expression of CD80$^+$, CD86$^+$ and MHC-II in CD19$^+$CD138$^-$ or CD19$^+$CD138$^+$ cells (Supplementary Fig. 12B). Therefore, we tested whether anti-IL6R treatment interfered with the ability of purified B cells (from Day 8 p.i.) to be activated upon *in vitro* stimulation with AQP4$_{201–220}$ or anti-CD40 antibody. Interestingly, while AQP4$_{201–220}$ did not elicit any significant changes in the expression of B-cell activation markers or IL-6 secretion, B cells from the anti-IL6R-treated group were less responsive to anti-CD40 stimulation compared with controls. At 24 and 72 h, these B cells exhibited significantly reduced expression of CD80 (24.3% and 16.4% reduction, respectively), CD86 (22.8% and 22.6% reduction, respectively) and MHC-II (27.3% and 57.3% reduction, respectively) and secreted significantly lower levels of IL-6 at 72 h (45% reduction) (Fig. 7D and E and Supplementary Fig. 12C). Consequently, IL-6 signalling is required for sustained activation of B cells and their differentiation into plasma cells.[63,66]

Finally, we addressed the importance of B cells in controlling Th17 differentiation via IL-6R signalling. B cells purified from anti-IL6R-treated IFNGRKO mice (Day 8 p.i.) were also relatively less potent in inducing Th17 differentiation if co-cultured with CD4$^+$ T cells in the presence of AQP4$_{201–220}$-peptide (29% lower Th17 frequency) (Fig. 7F). Administration of IL-6 to these co-cultures failed to increase the Th17 frequencies, which contrasted with the responses of the control B cells (1.49-fold increase). This apparent hypoactive state of B cells following *in vivo* anti-IL-6R treatment was restored only after polyclonal B-cell stimulation with anti-CD40 antibody (Fig. 7G). Similarly, CD4$^+$RORγ$^+$ T cell induction was suppressed in the same B-cell cultures (23.4% lower frequency) and failed to recover upon IL-6 administration, while CD4$^+$GM-CSF$^+$ T-cell and T_{reg} frequencies were not significantly affected (Supplementary Fig. 12D).

Tolerance induced by antigen-coupled PLGA nanoparticles ameliorates AQP4$_{201–220}$-induced disease

Lastly, we tested if AQP4$_{201–220}$-induced disease was susceptible to tolerogenic immunotherapy using antigen-coupled PLGA nanoparticles.[67-70] AQP4$_{201–220}$- or OVA$_{323–339}$-coupled PLGA nanoparticles were administered prophylactically at Day –7 p.i. or therapeutically at symptom onset to AQP4$_{201–220}$-immunized WT (also treated with anti-IFN-γ antibody) and IFNGRKO mice (Fig. 8A, D, H and I). Prophylactic administration of PLGA-AQP4$_{201–220}$ almost completely prevented the disease in both immunized groups. Clinical

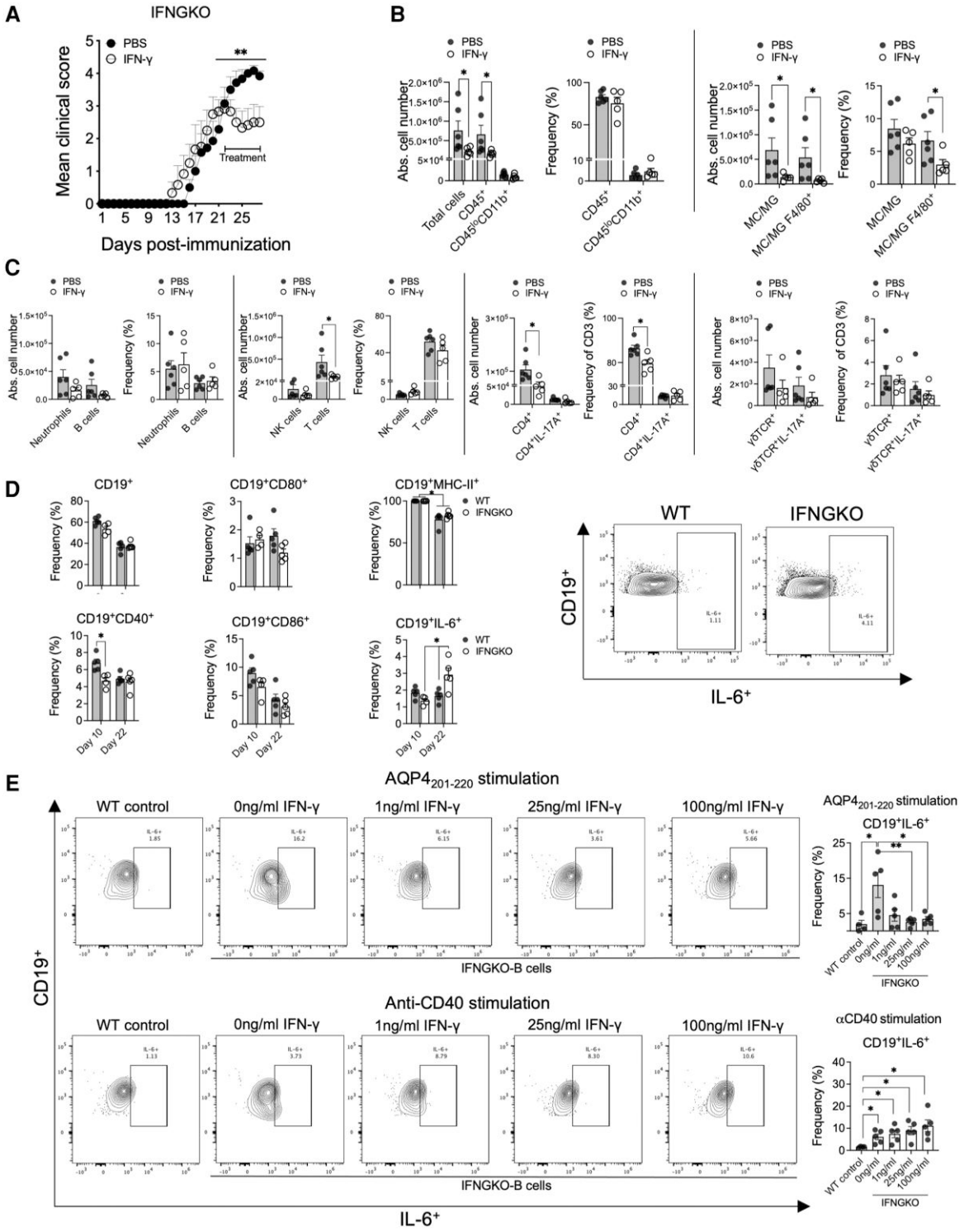

Figure 5 IFN-γ treatment reduces clinical severity and CNS inflammatory cell infiltration in IFN-γ knockout (IFNGKO) mice with AQP4$_{201-220}$-induced disease. Mean clinical scores of AQP4$_{201-220}$-immunized IFNGKO mice treated daily with recombinant IFN-γ (open circles, $n = 5$) or PBS (filled circles, $n = 6$) starting at the peak of the disease (Day 21) (**A**). Absolute cell numbers of total CNS mononuclear cells, CD45$^+$ cells and CD45^{lo}CD11b$^+$ cells (analysed by flow cytometry) for IFN-γ-treated (open circles) ($n = 6$) or PBS-treated (filled circles) ($n = 5$) mice (**B**). Absolute cell number and frequencies of monocytes/macrophages (MC)/activated microglia (MG;CD45^{hi}), MC/MGF4/80$^+$, Neutrophils Ly6G$^+$, NK (NK1.1$^+$), CD3$^+$, CD4$^+$, CD4$^+$17A$^+$, γδTCR$^+$, γδTCR$^+$IL-17A$^+$ and CD19$^+$ cells were determined by flowcytometry analyses (**C**). Flow cytometry frequency analysis of expression of activation markers (CD40, CD80, CD86, MHC-II and IL-6) on CD19$^+$ cells at Days 10 and 22 post-immunization (p.i.) in wild-type (WT) ($n = 5$) and IFNGKO ($n = 5$) AQP4$_{201-220}$-immunized mice (**D**). Pan-B cells purified from spleens of IFNGKO mice stimulated with 40 μg/ml AQP4$_{201-220}$ peptide or 1 μg/ml of coated anti-CD40 antibody for 72 h, with 0, 1, 25 and 100 ng/ml of IFN-γ. Frequencies of CD19$^+$IL-6$^+$ B cells were determined (**E**).WT pan-B cells were used as controls. All data are presented as mean ± SEM. Statistical analyses were performed using the Mann-Whitney test: $^*P < 0.05$, $^{**}P < 0.01$.

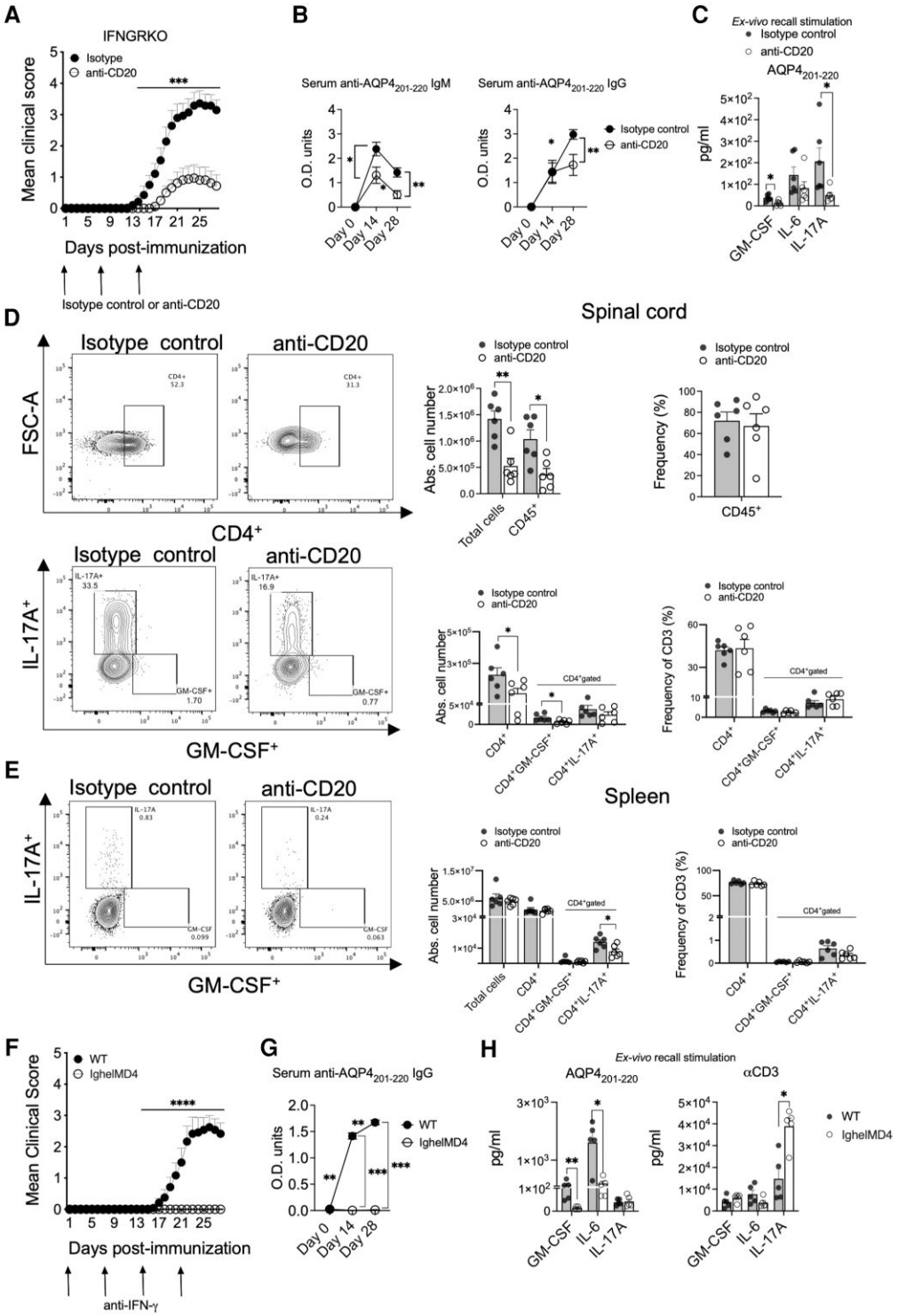

Figure 6 $AQP4_{201–220}$-induced disease is strictly dependent on B-cell activation. Mean clinical scores of $AQP4_{201–220}$-immunized IFN-γ-receptor knock-out (IFNGRKO) mice treated with three weekly doses of anti-CD20 (open circles, $n = 16$) or isotype control (filled circles, $n = 14$) antibodies starting at Day 0 (**A**). Optical density of total serum $AQP4_{201–220}$-specific IgM and IgG of mice treated with anti-CD20 (open circles, $n = 8$) or isotype control (filled circles, $n = 6$) antibodies were determined by ELISA at Days 0, 14 and 28 post-immunization (p.i.) (**B**). *Ex vivo* recall analysis (multiplex cytokine analysis) for GM-CSF, IL-6 and IL-17 of supernatants of splenocytes obtained from anti-CD20-treated ($n = 6$) and isotype control-treated ($n = 6$) mice at Day 28 p.i. and cultured for 72 h with 20 μg/ml $AQP4_{201–220}$ peptide (**C**). Flow cytometry analysis of the absolute cell numbers and frequency of $CD4^+$, $CD4^+GM\text{-}CSF^+$ and $CD4^+IL\text{-}17A^+$ T cells from the CNS (**D**) and spleen (**E**) of anti-CD20-treated ($n = 6$) or isotype control-treated ($n = 6$) mice. Mean clinical score of IghelMD4 ($n = 10$) and wild-type (WT) ($n = 12$) mice immunized and treated with weakly doses of anti-IFN-γ (**F**). Optical density of ELISA of total serum $AQP4_{201–220}$-specific IgG for IghelMD4 ($n = 6$) and WT ($n = 10$) mice at Days 0, 14 and 28 p.i (**G**). *Ex vivo* recall analysis (multiplex cytokine analysis) for GM-CSF, IL-6, and IL-17A of supernatants of splenocytes obtained from IghelMD4 ($n = 5$) and WT ($n = 5$) mice at Day 28 p.i. and cultured for 72 h with 40 μg/ml $AQP4_{201–220}$ peptide or 1 μg/ml of soluble anti-CD3 antibody (**H**). All data are presented as mean ± SEM. Statistical analyses were performed using the Mann–Whitney test. $^*P < 0.05$, $^{**}P < 0.01$, $^{***}P < 0.001$.

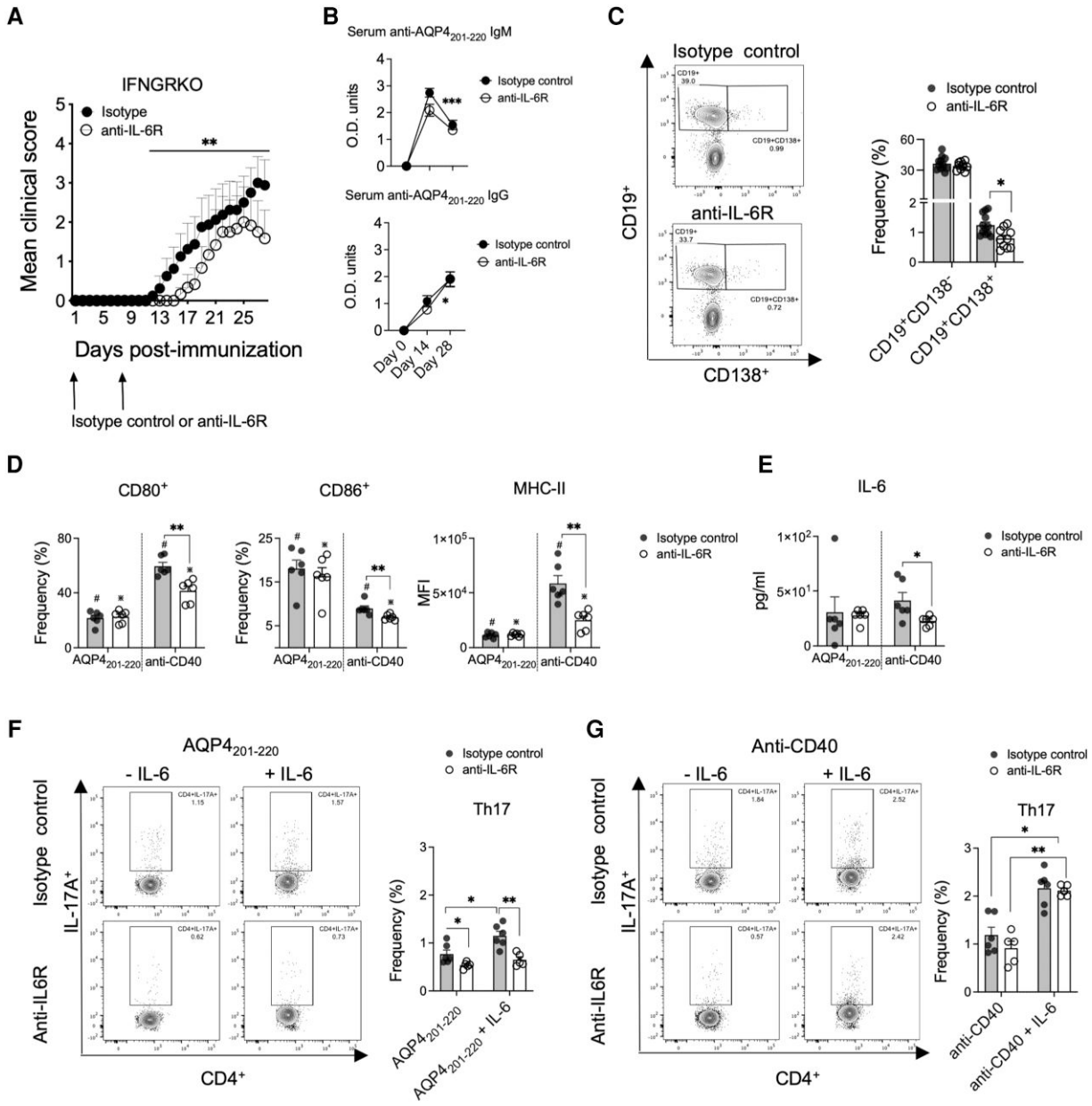

Figure 7 IL-6 signalling regulates severity of AQP4$_{201–220}$-induced disease and modulates B-cell activation and induction of Th17 cells. Mean clinical scores of AQP4$_{201–220}$-immunized IFN-γ-receptor knockout (IFNGRKO) mice treated with two weekly doses of anti-IL-6R (open circles, $n = 10$) or isotype control antibody (filled circles, $n = 13$) starting at Day 0 (**A**). Optical density of total serum anti-AQP4$_{201–220}$-specific IgM and IgG of mice treated with anti-IL6R (open circles, $n = 6$) or isotype control (filled circles, $n = 8$) antibodies were determined by ELISA at Days 0, 14 and 28 post-immunization (p.i.) (**B**). Flow cytometry frequency analysis of spleen CD19$^+$CD138$^+$ and CD19$^+$CD138$^-$ cells at Day 8 p.i. from mice treated with anti-IL6R (open circles, $n = 10$) and isotype control (filled circles, $n = 12$) antibodies (**C**). Flow cytometry frequency analysis of total CD19$^+$ pan-B cells purified at Day 8 p.i. from spleens of anti-IL6R ($n = 6$)- or isotype control ($n = 6$)-treated mice stimulated with 40 μg/ml of AQP4$_{201–220}$ peptide or 1 μg/ml of coated anti-CD40 for 72 h. Frequencies of CD80$^+$ and CD86$^+$ B cells, and MFI of MHC-II (**D**), as well as supernatant levels of IL-6 (measured by multiplex cytokine assay) (**E**) were determined. B cells stimulated for 24 h with either AQP4$_{201–220}$ peptide (**F**) or anti-CD40 (**G**) were washed and replated with untouched purified CD4$^+$ T cells from IFNGRKO mice at Day 9 p.i. at 1:1 ratio, with 0 or 10 ng/ml of recombinant IL-6 and cultured for 72 h, and the frequency of Th17 cells was assessed. All data are presented as mean ± SEM. Statistical analyses were performed using the Mann–Whitney test. $^*P < 0.05$, $^{**}P < 0.01$.

disease was observed in only 2/16 (12.5%) of the anti-IFN-γ-treated mice versus 13/16 (81.3%) of those that received PLGA-OVA$_{323–339}$. No clinical disease was observed in the IFNGRKO mice (0/5 affected) receiving PLGA-AQP4$_{201–220}$ prophylactically compared with the PLGA-OVA$_{323–339}$-treated controls (4/5 affected). Immunopathological analysis on WT and IFNGRKO treated mice demonstrated that disease prevention was associated with a significant reduction of serum AQP4$_{201–220}$ IgG levels (60 and 35% reduction, respectively), IL-17A secretion by splenocytes in *ex vivo* recall experiments (93% and 19% reduction, respectively) and inhibition of CNS inflammation (Fig. 8A–G and Supplementary Table 3A). Therapeutic treatment with PLGA-AQP4$_{201–220}$ also significantly decreased disease incidence (28%) and symptom severity (MCS = 0.5 at Day 31) in anti-IFN-γ-treated mice compared with PLGA-OVA$_{323–339}$ controls (57% incidence, MCS = 2.38) (Fig. 8H and I and Supplementary Table 3B). Similarly, administration of PLGA-AQP4$_{201–220}$ significantly reduced disease incidence in

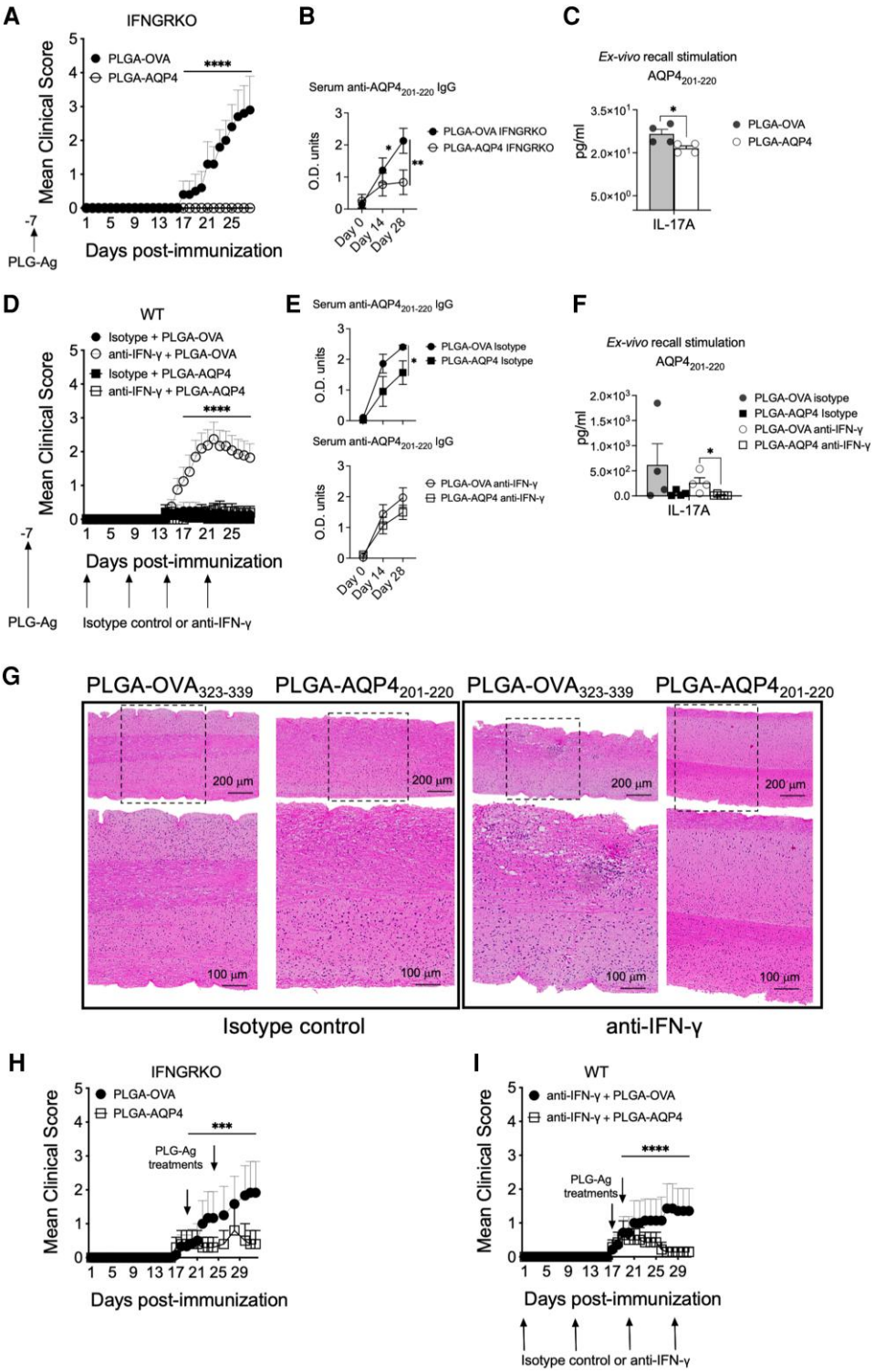

Figure 8 Immune tolerization by AQP4$_{201–220}$-coupled PLGA nanoparticles both prevents and ameliorates established AQP4$_{201–220}$-induced disease. Mean clinical scores of AQP4$_{201–220}$-immunized IFN-γ-receptor knockout (IFNGRKO) (**A** and **H**) and anti-IFN-γ-treated wild-type (WT) (**D** and **I**) mice receiving prophylactic intravenous infusion of either PLGA-AQP4$_{201–220}$ (PLGA-AQP4) or PLGA-OVA$_{323–339}$ (PLGA-OVA) nanoparticles 7 days prior to AQP4$_{201–220}$ immunization (Day −7) (**A** and **D**), or two therapeutic doses of nanoparticles at disease onset [Days 17–18 and Days 19–22 post-immunization (p.i.)] (**H** and **I**). See Supplementary Table 3 for the number of mice in each treatment group. Representative images of haematoxylin and eosin staining of lumbar spinal cord of isotype control- and anti-IFN-γ-treated WT mice that have received a prophylactic treatment with either PLGA-AQP4$_{201–220}$ or PLGA-OVA$_{323–339}$ 7 days prior to immunization (**G**). Serum anti-AQP4$_{201–220}$ IgG was measured by ELISA (**B** and **E**) and IL-17A secretion by splenocytes in *ex vivo* recall experiments quantitated by using multiplex cytokine assays (**C** and **F**). All data presented as mean ± SEM. Statistical analyses were performed using the Mann–Whitney test. ***$P < 0.001$, ****$P < 0.0001$. PLGA = poly(lactic-co-glycolic acid).

IFNGRKO mice (20% versus 60%) and the MCS at Day 31 p.i. (2.0 versus 3.83) compared to PLGA-OVA$_{323–339}$ treatment.

Discussion

Despite the recent advancements in understanding NMOSD, much remains unknown regarding the disease aetiology, pathogenesis and the mechanisms governing immune tolerance to AQP4. The need for novel non-immunosuppressive and curative treatments is still unmet. The objective barriers for further research are related to the fact that NMOSD is a rare idiopathic disorder, providing only limited opportunities for specimen collection, systematic investigation and clinical trials. Identifying the immunodominant epitopes of AQP4 that can elicit autoimmune responses in experimental animals raises the possibility of creating models based on active immunization and targeted manipulation of immune pathways.[21] However, the experimental strategies described thus far have failed to induce significant disease or trigger robust and sustained autoimmune inflammation of the CNS.[2,20,21,50,71]

The goal of the present study was to examine the potential role of IFN-γ in NMOSD and AQP4$_{201–220}$-induced disease. The principal result of the study is that NMOSD is characterized by decreased DEGs regulated by IFN-γ and that depletion of IFN-γ in AQP4$_{201–220}$-immunized C57BL/6 mice results in severe disease pathologically resembling NMOSD. Similar to NMOSD, IFN-β exacerbates the experimental disease.[22,23] The results further demonstrated that IFN-γ maintains natural immune tolerance to AQP4 by downregulating antigen-specific B-cell production of IL-6, induction of Th17 cells and by suppressing the transition of the initial autoimmune response into CNS inflammation and clinical disease. The effect of IFN-γ, although associated with the mechanisms of peripheral immune tolerance, appears to be T_{reg}-independent and related to controlling the expansion of self-reactive B and T cells. The study was a continuation of our prior work on the pleiotropic biological effects of IFN-γ and its role in CNS autoimmunity as well as on our earlier attempts to study NMOSD in animal models.[19,26,27,51,71–74]

Our initial hypothesis was based on an analysis of publicly available data on DEGs from whole blood of untreated NMOSD patients versus healthy controls.[7] Most of the identified DEGs were either dependent or co-dependent on IFN-γ, and those strictly linked to IFN-γ were predominantly downregulated. Recent reports have shown that *ifngr1*, *ifngr2* and *ifng* are downregulated DEGs, while expression of genes related to the Th17- and B-cell pathways are upregulated.[34] We found that disruption of IFN-γ, but not type I IFN, signalling led to significant CNS inflammation and severe paralytic disease in C57BL/6 mice. The clinical course of the disease was directly regulated by IFN-γ, controlling its incidence, severity and recovery. The inflammatory process involved the spinal cord and optic nerves and was characterized by T- and B-cell infiltration, antibody and complement deposition, as well as by significant loss of astrocytes and bystander injury to myelin, oligodendrocytes and neuronal axons. The process itself was driven by activated AQP4$_{201–220}$-specific B and Th17 cells and increased serum levels of AQP4 peptide- and AQP4 protein-specific autoantibodies. Overall, the AQP4$_{201–220}$-induced disease demonstrated significant immunological and clinicopathological similarities with NMOSD.[1]

This model shares additional immunopathologic and mechanistic features with NMOSD. For instance, we observed elevated numbers of neutrophils in the CNS and elevated levels of the neutrophil and monocyte/macrophage chemoattractants, all consistent with NMOSD pathology.[9,75] Similarly to NMOSD, we found IL-6 and IL-17 levels to be significantly increased following AQP4$_{201–220}$ immunization in the absence of IFN-γ.[7,30,32,62,76] We also observed significant upregulation of Th17-related genes (*il17a*, *rorc* and *cd4*) and increased numbers of total CD4$^+$ and Th17 cells in the CNS. Moreover, the receptor genes for IL-1ß (*il1r1*) and IL-6 (*il6st*) needed for Th17 differentiation were also upregulated.[77–79] Finally, the regulatory role of IFN-γ in AQP4$_{202–220}$-induced disease was supported by its ability to significantly ameliorate the disease and to reduce the numbers of CNS-infiltrating T cells upon administration to IFNGKO mice.

B cells promote NMOSD pathogenesis by differentiating into antibody-producing plasma cells, as well as via secretion of pro-inflammatory cytokines and by serving as antigen-presenting cells, facilitating Th17 differentiation.[18] The importance of the immunoregulatory functions of B cells in NMOSD is reflected in the success of anti-CD20 immunotherapy.[80,81] We found that priming with AQP4$_{201–220}$ in the absence of IFN-γ increased peripheral B-cell receptor signalling and the numbers of CD19 B cells infiltrating the CNS. Anti-CD20 treatment significantly ameliorated AQP4$_{201–220}$-induced disease, an effect associated with lower serum levels of anti-AQP4$_{201–220}$-specific antibodies and with reduction of total Th17 cells in the spleen, and CD4$^+$ and GM-CSF-expressing T cells in the CNS. Recall cultures demonstrated a decreased ability to produce IL-17 and GM-CSF, cytokines critical for driving experimental autoimmune encephalitis (EAE).[81,82] The ameliorative effective of anti-IL-17A treatment on the experimental disease, although less dramatic, provided additional support to the significance of the B cell–Th17 cell pathway.

The role of B cells in Th17-cell activation and differentiation is still unclear; however, it is likely to include IL-6 signalling.[7,83–85] Our results demonstrated that IFN-γ regulates B-cell expression of IL-6 in an antigen-specific fashion in AQP4$_{201–220}$-primed mice. Notably, anti-IFN-γ-treated IghelMD4 mice failed to display symptoms associated with lower spleen IL-6 secretion. Moreover, blockade of IL-6 signalling in AQP4$_{201–220}$-induced disease significantly decreased the frequency of splenic plasma cells and serum anti-AQP4$_{201–220}$ IgM titres. B cells from the anti-IL-6R-treated mice were unable to induce Th17 differentiation and to upregulate activation makers. This is also observed in NMOSD patients treated with anti-IL-6R antibody, wherein the frequency of B and plasma cells, levels of B cell costimulatory molecule expression and Th17 differentiation are diminished.[17] Collectively, our results demonstrate that in the absence of IFN-γ, disease outcomes are fully dependent on B cells and their activation, indicating that IFN-γ plays a critical role in regulating the interplay between pathogenic AQP4$_{201–220}$-specific B and Th17 cells.

We also tested if our NMOSD model could serve as a relevant platform for the development and testing of immune therapies. Two of the three monoclonal antibodies currently used therapeutically in NMOSD, anti-CD20 and anti-IL-6R were tested in our model. Both treatments significantly reduced the incidence and severity of the AQP4$_{201–220}$-induced disease. We also demonstrated that administration of recombinant IFN-γ and anti-IL-17A antibody, both with commercial analogues and currently in clinical use for the treatment of rheumatological disorders [ACTIMMUNE® (Horizon Pharma) and COSENTYX® (Novartis), respectively][86,87] reduced clinical progression and re-established immune homeostasis. It is conceivable that selected NMOSD patients with decreased levels of IFN-γ gene expression or elevated levels of IL-17A might benefit from these treatments. Further research of the IFN-γ signalling pathway might identify novel therapeutic targets related to the regulation of Th17 and B cell responses, maintenance of immune tolerance and CNS inflammation.

Our laboratory has developed an immune tolerance induction methodology using carboxylated, biodegradable nanoparticles composed of the US Food and Drug Administration-approved polymer PLGA to encapsulate proteins/peptides for the prevention and treatment of myelin peptide-induced EAE and spontaneous type 1 diabetes, and tested these in a phase 1/2a clinical trial in coeliac disease patients.[67-70,88] Like coeliac disease, NMOSD may benefit from this tolerogenic therapy, as the autoimmune response to AQP4 is the primary immunopathologic feature. We demonstrated in our NMOSD model that tolerization with PLGA-AQP4$_{201–220}$ nanoparticles significantly suppressed induction (prophylactic treatment) and progression (therapeutic treatment) of the clinical disease in both anti-IFN-γ-treated WT and IFNGRKO mice. Disease amelioration was associated with a significant reduction of the serum levels of anti-AQP4 antibodies, secretion of IL-17A in recall assays and inhibition of CNS inflammation. Noting that PLGA-AQP4$_{201–220}$-induced tolerance occurs in the absence of IFN-γ indicates that immune tolerance can overcome the type I/type II IFN disbalance of the experimental disease and that the immunoregulatory effects of IFN are likely broader in scope.[67-70] Collectively, these results suggest that AQP4-specific tolerance could be a promising treatment strategy for NMOSD because of its novel mechanism of action, potential wide-ranging efficacy and absence of immunosuppressive side effects.[19]

Limitations of our disease model should be taken into consideration when interpreting our results in comparison to NMOSD. The experimental disease is based on active immunization and breakdown of immune tolerance to AQP4 using an IFN-γ signalling blockade, which resulted in acute inflammation and significant clinical disease. The clinicopathological characteristics of our model more closely resemble the acute progressive monophasic form of NMOSD; thus, it does not fully represent the clinical spectrum of the human disease.[89] CNS lesions were oedematous and dominated by cellular infiltration that might overshadow direct and complement-mediated cytopathic effects of anti-AQP4 antibody, creating more restricted pathological patterns that only partially reproduce the heterogeneity of NMOSD pathology or patterns observed in other experimental models. The appearance of anti-AQP4 IgG in our model lags behind the cellular immune response which, in addition to the potential species differences in complement activity, may also contribute to some of the clinicopathological dissimilarities.[90,91] The goal of our future experiments is to generate a more chronic-relapsing disease by re-dosing the anti-IFN-γ treatments to allow for longitudinal, immunological and cell-focused studies. Both IFN-γ signalling regulation of B-cell activity and immune tolerance to AQP4 need to be explored at the single-cell level. Finally, the experiments demonstrating the beneficial effect of PLGA-AQP4$_{201–220}$ on our disease model will be expanded to include tolerance to native APQ4 protein and preclinical trial designs.

In conclusion, this study shows for the first time the critical role of IFN-γ as a master regulator of immunopathologic AQP4-specific B and Th17 cell responses as well as autoantibody levels and its essential involvement in natural immune tolerance. Our animal model of NMOSD can serve as a clinically relevant platform to further study pathological mechanisms of disease and to screen novel immunologic and cell protective therapies.

Data availability

The authors confirm that the data supporting the findings of this study are available within the article and its Supplementary material.

Acknowledgements

We thank the members of the Miller, Balabanov, Popko and Chen labs for their helpful suggestions. We thank Guthy Jackson Charitable Foundation and Dr Robert Stroud (UCSF) for kindly providing the recombinant human AQP4 protein.

Funding

This work was supported by National Institute of Neurological Disorders and Stroke grants R21AI151438 and R01 NS099334 and by gifts from the Johnnie Walkers MS Foundation, the Amy and David Fulton Foundation, the Crammer Family Foundation, the Thomas and Deige McLaughlin Foundation and the Rottering Family Foundation. T.N. was supported by a JDRF Postdoctoral Fellowship 3-PDF-2018-582-A-N. Y.C. was supported by the National Multiple Sclerosis Society Career Transition Fellowship TA-2008-37043. B.P. was supported by NIH/NINDS R01 NS034939, the Dr Miriam and Sheldon G Adelson Medical Research Foundation and the Rampy MS Research Foundation.

Competing interests

S.D.M. is an academic co-founder, scientific advisory board member, paid consultant and grantee of COUR Pharmaceuticals and a consultant for NextCure and Takeda Pharmaceuticals. J.R.P. is an employee of COUR Pharmaceuticals. R.B. has received honoraria from Biogen, Teva Pharmaceuticals, Sanofi and Alexion. B.P. is a member of the scientific advisory board of Inflectis Bioscience. The other authors report no competing interests.

Supplementary material

Supplementary material is available at *Brain* online.

References

1. Jarius S, Paul F, Weinshenker BG, Levy M, Kim HJ, Wildemann B. Neuromyelitis optica. *Nat Rev Dis Primers*. 2020;6:85.
2. Varrin-Doyer M, Spencer CM, Schulze-Topphoff U, et al. Aquaporin 4-specific T cells in neuromyelitis optica exhibit a Th17 bias and recognize clostridium ABC transporter. *Ann Neurol*. 2012;72:53-64.
3. Carnero Contentti E, Correale J. Neuromyelitis optica spectrum disorders: From pathophysiology to therapeutic strategies. *J Neuroinflammation*. 2021;18:208.
4. Saadoun S, Waters P, Bell BA, Vincent A, Verkman AS, Papadopoulos MC. Intra-cerebral injection of neuromyelitis optica immunoglobulin G and human complement produces neuromyelitis optica lesions in mice. *Brain*. 2010;133(Pt 2):349-361.
5. Pohl M, Kawakami N, Kitic M, et al. T cell-activation in neuromyelitis optica lesions plays a role in their formation. *Acta Neuropathol Commun*. 2013;1:85.
6. Hinson SR, McKeon A, Fryer JP, Apiwattanakul M, Lennon VA, Pittock SJ. Prediction of neuromyelitis optica attack severity by quantitation of complement-mediated injury to aquaporin 4-expressing cells. *Arch Neurol*. 2009;66:1164-1167.
7. Agasing AM, Wu Q, Khatri B, et al. Transcriptomics and proteomics reveal a cooperation between interferon and T-helper 17 cells in neuromyelitis optica. *Nat Commun*. 2020;11:2856.

8. Duan T, Smith AJ, Verkman AS. Complement-dependent bystander injury to neurons in AQP4-IgG seropositive neuromyelitis optica. *J Neuroinflammation*. 2018;15:294.
9. Saadoun S, Waters P, MacDonald C, et al. Neutrophil protease inhibition reduces neuromyelitis optica-immunoglobulin G-induced damage in mouse brain. *Ann Neurol*. 2012;71:323-333.
10. Tradtrantip L, Yao X, Su T, Smith AJ, Verkman AS. Bystander mechanism for complement-initiated early oligodendrocyte injury in neuromyelitis optica. *Acta Neuropathol*. 2017;134: 35-44.
11. Guo Y, Lennon VA, Parisi JE, et al. Spectrum of sublytic astrocytopathy in neuromyelitis optica. *Brain*. 2021;145:1379-1390.
12. Takai Y, Misu T, Suzuki H, et al. Staging of astrocytopathy and complement activation in neuromyelitis optica spectrum disorders. *Brain*. 2021;144:2401-2415.
13. Shaygannejad V, Fayyazi E, Badihian S, et al. Long-term tolerability, safety and efficacy of rituximab in neuromyelitis optica spectrum disorder: A prospective study. *J Neurol*. 2019;266:642-650.
14. Tullman MJ, Zabeti A, Vuocolo S, Dinh Q. Inebilizumab for treatment of neuromyelitis optica spectrum disorder. *Neurodegener Dis Manag*. 2021;11:341-352.
15. Pittock SJ, Berthele A, Fujihara K, et al. Eculizumab in aquaporin 4–positive neuromyelitis optica spectrum disorder. *N Engl J Med*. 2019;381:614-625.
16. Araki M, Matsuoka T, Miyamoto K, et al. Efficacy of the anti-IL-6 receptor antibody tocilizumab in neuromyelitis optica: A pilot study. *Neurology*. 2014;82:1302-1306.
17. Liu Y, Zhang H, Zhang T-X, et al. Effects of tocilizumab therapy on circulating B cells and T helper cells in patients with neuromyelitis optica spectrum disorder. *Front Immunol*. 2021;12:703931.
18. Traub J, Husseini L, Weber MS. B cells and antibodies as targets of therapeutic intervention in neuromyelitis optica spectrum disorders. *Pharmaceuticals (Basel)*. 2021;14:37.
19. Loda E, Arellano G, Perez-Giraldo G, Miller SD, Balabanov R. Can immune tolerance be re-established in neuromyelitis optica? *Front Neurol*. 2021;12:783304.
20. Duan T, Verkman AS. Experimental animal models of aquaporin 4-IgG-seropositive neuromyelitis optica spectrum disorders: Progress and shortcomings. *Brain Pathol*. 2020;30:13-25.
21. Nelson PA, Khodadoust M, Prodhomme T, et al. Immunodominant T cell determinants of aquaporin 4, the autoantigen associated with neuromyelitis optica. *PLoS One*. 2010;5:e15050.
22. Kim S-H, Kim W, Li XF, Jung I-J, Kim HJ. Does interferon beta treatment exacerbate neuromyelitis optica spectrum disorder? *Mult Scler*. 2012;18:1480-1483.
23. Palace J, Leite MI, Nairne A, Vincent A. Interferon beta treatment in neuromyelitis optica: Increase in relapses and aquaporin 4 antibody titers. *Arch Neurol*. 2010;67:1016-1017.
24. Panitch HS, Hirsch RL, Schindler J, Johnson KP. Treatment of multiple sclerosis with gamma interferon: Exacerbations associated with activation of the immune system. *Neurology*. 1987; 37:1097-1102.
25. Naves R, Singh SP, Cashman KS, et al. The interdependent, overlapping, and differential roles of type I and II IFNs in the pathogenesis of experimental autoimmune encephalomyelitis. *J Immunol*. 2013;191:2967-2977.
26. Ottum PA, Arellano G, Reyes LI, Iruretagoyena M, Naves R. Opposing roles of interferon-gamma on cells of the central nervous system in autoimmune neuroinflammation. *Front Immunol*. 2015;6:539.
27. Arellano G, Ottum PA, Reyes LI, Burgos PI, Naves R. Stage-specific role of interferon-gamma in experimental autoimmune encephalomyelitis and multiple sclerosis. *Front Immunol*. 2015;6:492.
28. Axtell RC, de Jong BA, Boniface K, et al. T helper type 1 and 17 cells determine efficacy of interferon-beta in multiple sclerosis and experimental encephalomyelitis. *Nat Med*. 2010;16:406-412.
29. Arellano G, Acuña E, Reyes LI, et al. Th1 and Th17 cells and associated cytokines discriminate among clinically isolated syndrome and multiple sclerosis phenotypes. *Front Immunol*. 2017; 8:753.
30. Hou M-M, Li Y-F, He L-L, et al. Proportions of Th17 cells and Th17-related cytokines in neuromyelitis optica spectrum disorders patients: A meta-analysis. *Int Immunopharmacol*. 2019;75: 105793.
31. Li Y, Wang H, Long Y, Lu Z, Hu X. Increased memory Th17 cells in patients with neuromyelitis optica and multiple sclerosis. *J Neuroimmunol*. 2011;234:155-160.
32. Monteiro C, Fernandes G, Kasahara TM, et al. The expansion of circulating IL-6 and IL-17-secreting follicular helper T cells is associated with neurological disabilities in neuromyelitis optica spectrum disorders. *J Neuroimmunol*. 2019;330:12-18.
33. Liu J, Tan G, Li B, et al. Serum aquaporin 4-immunoglobulin G titer and neuromyelitis optica spectrum disorder activity and severity: A systematic review and meta-analysis. *Front Neurol*. 2021;12:746959.
34. Zhou Y, Song S, Han Y, et al. Altered non-coding RNA profiles and potential disease marker identification in peripheral blood mononuclear cells of patients with NMOSD. *Int Immunopharmacol*. 2022; 109:108899.
35. Wang KC, Lee C-L, Chen S-Y, et al. Distinct serum cytokine profiles in neuromyelitis optica and multiple sclerosis. *J Interferon Cytokine Res*. 2013;33:58-64.
36. Wang K-C, Tsai C-P, Lee C-L, Chen S-Y, Chin L-T, Chen S-J. Elevated plasma high-mobility group box 1 protein is a potential marker for neuromyelitis optica. *Neuroscience*. 2012;226: 510-516.
37. Ghafouri-Fard S, Azimi T, Taheri M. A comprehensive review on the role of genetic factors in neuromyelitis optica spectrum disorder. *Front Immunol*. 2021;12:737673.
38. Matsushita T, Tateishi T, Isobe N, et al. Characteristic cerebrospinal fluid cytokine/chemokine profiles in neuromyelitis optica, relapsing remitting or primary progressive multiple sclerosis. *PLoS One*. 2013;8:e61835.
39. Uzawa A, Mori M, Ito M, et al. Markedly increased CSF interleukin-6 levels in neuromyelitis optica, but not in multiple sclerosis. *J Neurol*. 2009;256:2082-2084.
40. Xu W, Li R, Dai Y, et al. IL-22 secreting CD4+ T cells in the patients with neuromyelitis optica and multiple sclerosis. *J Neuroimmunol*. 2013;261:87-91.
41. Kwon YN, Kim B, Ahn S, et al. Serum level of IL-1β in patients with inflammatory demyelinating disease: Marked upregulation in the early acute phase of MOG antibody associated disease (MOGAD). *J Neuroimmunol*. 2020;348:577361.
42. Ulusoy C, Tüzün E, Kürtüncü M, Türkoğlu R, Akman-Demir G, Eraksoy M. Comparison of the cytokine profiles of patients with neuronal-antibody-associated central nervous system disorders. *Int J Neurosci*. 2012;122:284-289.
43. Pentón-Rol G, Cervantes-Llanos M, Martínez-Sánchez G, et al. TNF-α and IL-10 downregulation and marked oxidative stress in neuromyelitis optica. *J Inflamm*. 2009;6:18.
44. Huang S, Hendriks W, Althage A, et al. Immune response in mice that lack the interferon-gamma receptor. *Science*. 1993; 259:1742-1745.
45. Ferber IA, Brocke S, Taylor-Edwards C, et al. Mice with a disrupted IFN-gamma gene are susceptible to the induction of experimental autoimmune encephalomyelitis (EAE). *J Immunol*. 1996;156:5-7.

46. Müller U, Steinhoff U, Reis LF, et al. Functional role of type I and type II interferons in antiviral defense. *Science*. 1994;264:1918-1921.
47. Kim JM, Rasmussen JP, Rudensky AY. Regulatory T cells prevent catastrophic autoimmunity throughout the lifespan of mice. *Nat Immunol*. 2007;8:191-197.
48. Mason DY, Jones M, Goodnow CC. Development and follicular localization of tolerant B lymphocytes in lysozyme/anti-lysozyme IgM/IgD transgenic mice. *Int Immunol*. 1992;4:163-175.
49. Kitaura H, Tsujita M, Huber VJ, et al. Activity-dependent glial swelling is impaired in aquaporin 4 knockout mice. *Neurosci Res*. 2009;64:208-212.
50. Sagan SA, Winger RC, Cruz-Herranz A, et al. Tolerance checkpoint bypass permits emergence of pathogenic T cells to neuromyelitis optica autoantigen aquaporin 4. *Proc Natl Acad Sci U S A*. 2016;113:14781-14786.
51. Tichauer JE, Arellano G, Acuña E, et al. Interferon-gamma ameliorates experimental autoimmune encephalomyelitis by inducing homeostatic adaptation of microglia. *Front Immunol*. 2023;14:1191838.
52. González LF, Acuña E, Arellano G, et al. Intranasal delivery of interferon-β-loaded nanoparticles induces control of neuroinflammation in a preclinical model of multiple sclerosis: A promising simple, effective, non-invasive, and low-cost therapy. *J Control Release*. 2021;331:443-459.
53. Dorrier CE, Aran D, Haenelt EA, et al. CNS fibroblasts form a fibrotic scar in response to immune cell infiltration. *Nat Neurosci*. 2021;24:234-244.
54. Robinson AP, Rodgers JM, Goings GE, Miller SD. Characterization of oligodendroglial populations in mouse demyelinating disease using flow cytometry: Clues for MS pathogenesis. *PLoS One*. 2014;9:e107649.
55. Podojil JR, Liu LN, Marshall SA, et al. B7-H4Ig inhibits mouse and human T-cell function and treats EAE via IL-10/Treg-dependent mechanisms. *J Autoimmun*. 2013;44:71-81.
56. Rusinova I, Forster S, Yu S, et al. INTERFEROME V2.0: An updated database of annotated interferon-regulated genes. *Nucleic Acids Res*. 2012;41:D1040-D1046.
57. Gillespie M, Jassal B, Stephan R, et al. The reactome pathway knowledgebase 2022. *Nucleic Acids Res*. 2021;50:D687-D692.
58. Vogel AL, Knier B, Lammens K, et al. Deletional tolerance prevents AQP4-directed autoimmunity in mice. *Eur J Immunol*. 2017;47:458-469.
59. Sun W, Cornwell A, Li J, et al. SOX9 is an astrocyte-specific nuclear marker in the adult brain outside the neurogenic regions. *J Neurosci*. 2017;37:4493-4507.
60. Escartin C, Galea E, Lakatos A, et al. Reactive astrocyte nomenclature, definitions, and future directions. *Nat Neurosci*. 2021;24:312-325.
61. Lin J, Zhou L, Luo Z, et al. Flow cytometry analysis of immune and glial cells in a trigeminal neuralgia rat model. *Sci Rep*. 2021;11:23569.
62. Maciak K, Pietrasik S, Dziedzic A, et al. Th17-related cytokines as potential discriminatory markers between neuromyelitis optica (Devic's disease) and multiple sclerosis-a review. *Int J Mol Sci*. 2021;22:8946.
63. Chihara N, Aranami T, Sato W, et al. Interleukin 6 signaling promotes anti-aquaporin 4 autoantibody production from plasmablasts in neuromyelitis optica. *Proc Natl Acad Sci U S A*. 2011;108:3701-3706.
64. Estrada K, Whelan CW, Zhao F, et al. A whole-genome sequence study identifies genetic risk factors for neuromyelitis optica. *Nat Commun*. 2018;9:1929.
65. Lubbers R, van Essen MF, van Kooten C, Trouw LA. Production of complement components by cells of the immune system. *Clin Exp Immunol*. 2017;188:183-194.
66. Kawano MM, Mihara K, Huang N, Tsujimoto T, Kuramoto A. Differentiation of early plasma cells on bone marrow stromal cells requires interleukin-6 for escaping from apoptosis. *Blood*. 1995;85:487-494.
67. Podojil JR, Genardi S, Chiang M-Y, et al. Tolerogenic immune-modifying nanoparticles encapsulating multiple recombinant pancreatic β cell proteins prevent onset and progression of type 1 diabetes in nonobese diabetic mice. *J Immunol*. 2022;209:465-475.
68. Freitag TL, Podojil JR, Pearson RM, et al. Gliadin nanoparticles induce immune tolerance to gliadin in mouse models of celiac disease. *Gastroenterology*. 2020;158:1667-1681.e12.
69. Getts DR, Martin AJ, McCarthy DP, et al. Microparticles bearing encephalitogenic peptides induce T-cell tolerance and ameliorate experimental autoimmune encephalomyelitis. *Nat Biotechnol*. 2012;30:1217-1224.
70. Hunter Z, McCarthy DP, Yap WT, et al. A biodegradable nanoparticle platform for the induction of antigen-specific immune tolerance for treatment of autoimmune disease. *ACS Nano*. 2014;8:2148-2160.
71. Ren Z, Wang Y, Duan T, et al. Cross-immunoreactivity between bacterial aquaporin-Z and human aquaporin-4: Potential relevance to neuromyelitis optica. *J Immunol*. 2012;189:4602-4611.
72. Balabanov R, Strand K, Goswami R, et al. Interferon-gamma-oligodendrocyte interactions in the regulation of experimental autoimmune encephalomyelitis. *J Neurosci*. 2007;27:2013-2024.
73. Chen Y, Kunjamma RB, Weiner M, Chan JR, Popko B. Prolonging the integrated stress response enhances CNS remyelination in an inflammatory environment. *Elife*. 2021;10:e65469.
74. Lin W, Kunkler PE, Harding HP, Ron D, Kraig RP, Popko B. Enhanced integrated stress response promotes myelinating oligodendrocyte survival in response to interferon-gamma. *Am J Pathol*. 2008;173:1508-1517.
75. Kobayashi S, Kokubun N, Aoki R, Hamaguchi M, Matsuda H, Suzuki K. Possible role of neutrophils in astrocyte injury in neuromyelitis optica spectrum disorder. *J Neurol Sci*. 2022;438:120293.
76. Yeh W-I, McWilliams IL, Harrington LE. IFNγ inhibits Th17 differentiation and function via Tbet-dependent and Tbet-independent mechanisms. *J Neuroimmunol*. 2014;267:20-27.
77. Mailer RKW, Joly A-L, Liu S, Elias S, Tegner J, Andersson J. IL-1β promotes Th17 differentiation by inducing alternative splicing of FOXP3. *Sci Rep*. 2015;5:14674.
78. Sha Y, Markovic-Plese S. A role of IL-1R1 signaling in the differentiation of Th17 cells and the development of autoimmune diseases. *Self Nonself*. 2011;2:35-42.
79. Harbour SN, DiToro DF, Witte SJ, et al. T(H)17 cells require ongoing classic IL-6 receptor signaling to retain transcriptional and functional identity. *Sci Immunol*. 2020;5:eaaw2262.
80. Wang Y, Chang H, Zhang X, Yin L. Efficacy of rituximab in the treatment of neuromyelitis optica spectrum disorders: An update systematic review and meta-analysis. *Mult Scler Relat Disord*. 2021;50:102843.
81. Croxford AL, Lanzinger M, Hartmann FJ, et al. The cytokine GM-CSF drives the inflammatory signature of CCR2+ monocytes and licenses autoimmunity. *Immunity*. 2015;43:502-514.
82. Ifergan I, Davidson TS, Kebir H, et al. Targeting the GM-CSF receptor for the treatment of CNS autoimmunity. *J Autoimmun*. 2017;84:1-11.
83. Bennett JL, O'Connor KC, Bar-Or A, et al. B lymphocytes in neuromyelitis optica. *Neurol Neuroimmunol Neuroinflamm*. 2015;2:e104.
84. Barr TA, Shen P, Brown S, et al. B cell depletion therapy ameliorates autoimmune disease through ablation of IL-6-producing B cells. *J Exp Med*. 2012;209:1001-1010.

85. Agasing AM, Gawde S, Kumar G, Turner E, Axtell RC. B cell function impacts the efficacy of IFN-β therapy in EAE. *J Neuroimmunol*. 2020;338:577106.
86. US Food and Drug Administration. Actimmune® (interferon gamma-1b) injection, for subcutaneous use. Initial U.S. Approval: 1990. Reference ID: 3812499. https://www.accessdata.fda.gov/drugsatfda_docs/label/2015/103836s5182lbl.pdf
87. US Food and Drug Administration. Cosentyx® (secukinumab) injection, for subcutaneous use. Initial U.S. Approval: 2015. Reference ID: 3874646. https://www.accessdata.fda.gov/drugsatfda_docs/label/2016/125504s001s002lbl.pdf
88. Kelly CP, Murray JA, Leffler DA, et al. TAK-101 nanoparticles induce gluten-specific tolerance in celiac disease: A randomized, double-blind, placebo-controlled study. *Gastroenterology*. 2021;161:66-80.e8.
89. Lucchinetti CF, Guo Y, Popescu BF, Fujihara K, Itoyama Y, MisuT. The pathology of an autoimmune astrocytopathy: Lessons learned from neuromyelitis optica. *Brain Pathol*. 2014;24:83-97.
90. Geis C, Ritter C, Ruschil C, et al. The intrinsic pathogenic role of autoantibodies to aquaporin 4 mediating spinal cord disease in a rat passive-transfer model. *Exp Neurol*. 2015;265:8-21.
91. Hillebrand S, Schanda K, Nigritinou M, et al. Circulating AQP4-specific auto-antibodies alone can induce neuromyelitis optica spectrum disorder in the rat. *Acta Neuropathol*. 2019;137:467-485.